AN ABSTRACT OF THE THESIS OF

Maribel Gómez Rios for the degree of Master of Science in Physics presented on May 7 1999. Title: Thermal Neutron Capture Cross Sections of ^{68}Ge and ^{148}Gd.

Abstract approved: Redacted for Privacy

Kenneth S. Krane

Radiative capture is one of the processes that can occur when a neutron interacts with a nucleus. Thermal neutron capture cross sections (σ_c) can be used to explain fundamental principles of nuclear structure as well as observations in stellar nucleosynthesis. Neutron capture spectra also have been applied in biomedicine, environmental studies, and archeology. Although extensive studies have been conducted to determine the σ_c of stable nuclei, much less information is available about the σ_c of radioactive elements. In these experiments, radioactive sources of ^{68}Ge and ^{148}Gd were irradiated by thermal neutrons in a reactor. The γ-ray energy spectra of the resultant ^{69}Ge and ^{149}Gd isotopes were observed and used to calculate the σ_c for both. Medium- and heavy-mass stable nuclei are known to exhibit typical σ_c values from 10^0 to 10^3 b. The results of this analysis show that the σ_c of ^{68}Ge is at the very low end of this range at 1.03 ± 0.51 b and that the σ_c of ^{148}Gd is higher than this range at about 1.41×10^4 b. Upper limits of the (n,p) and (n,α) cross sections for ^{148}Gd also are deduced.

Thermal Neutron Capture Cross Sections of ^{68}Ge and ^{148}Gd

by

Maribel Gómez Rios

A Thesis Submitted
to
Oregon State University

In Partial Fulfillment of
the requirements for the
degree of

Master of Science

Presented May 7, 1999
Commencement June 1999

Master of Science thesis of Maribel Gómez Rios presented on May 7 1999

Approved:

Redacted for Privacy

Major Professor, representing Physics

Redacted for Privacy

Chair of the Department of Physics

Redacted for Privacy

Dean of Graduate School

I understand that my thesis will become part of the permanent collection of Oregon State University libraries. My signature below authorizes release of my thesis to any reader upon request.

Redacted for Privacy

Maribel Gómez Rios, Author

ACKNOWLEDGMENT

I am indebted to the help and guidance of my major research professor, Dr. Ken Krane, as well as to the OSU Radiation Center for its professional service, Dr. Rick Norman for the purchase and careful preparation of each sample, Mike Dragowsky for his assistance with the figures, members of the examination committee for their time, the US Department of Energy for its support, and the faculty and staff at Oregon State University and the Oregon State University Physics Department.

On a personal note, I express my immense gratitude to my parents, Ramiro and Onorina Gómez, for their wisdom and invaluable teachings. Also, I would like to thank Ramiro Jr., Lisa, Marissa, Nelda, and Frank Gómez and Aurelio and Reynalda Rios and family. Finally, I extend a special recognition to my husband, Roberto, for his many years of unconditional love, understanding, support, and patience.

TABLE OF CONTENTS

TABLE OF CONTENTS, CONTINUED

LIST OF FIGURES

LIST OF TABLES

Thermal Neutron Capture Cross Sections of ^{68}Ge and ^{148}Gd

I. INTRODUCTION

Radiative capture is one of the interactions that can occur between a neutron and a nucleus. During neutron radiative capture, also known as an (n,γ) reaction, a target nucleus captures a neutron to become a heavier isotope of the same element. Symbolically,

$$n + {}^{A}X \longrightarrow {}^{A+1}X + \gamma$$

where n is the bombarding neutron, ^{A}X is the target nucleus, ^{A+1}X is the resultant nucleus, and γ is the emitted energy in the form of gamma radiation. In effect, the nucleus ^{A+1}X is formed in a highly excited state and decays quickly to its ground state by the emission of γ radiation.

The excitation energy in the form of γ radiation is equal to the sum of the energy of the bombarding particle and the neutron separation energy — the energy required to separate the neutron from the nucleus, which is equal to $[m(^{A+1}X) - m(^{A}X) - m(n)]c^2$ and is thus specific to the isotope [Lyn68]. This γ radiation is emitted very rapidly in the form of primary transitions of energies in the range of several MeV — which carry the nucleus ^{A+1}X from the capture state to its low-lying excited states — and subsequently in the form of secondary transitions of energies usually below 1 MeV — which take place between the low-lying excited states and eventually carry the nucleus to its ground state (Figure 1).

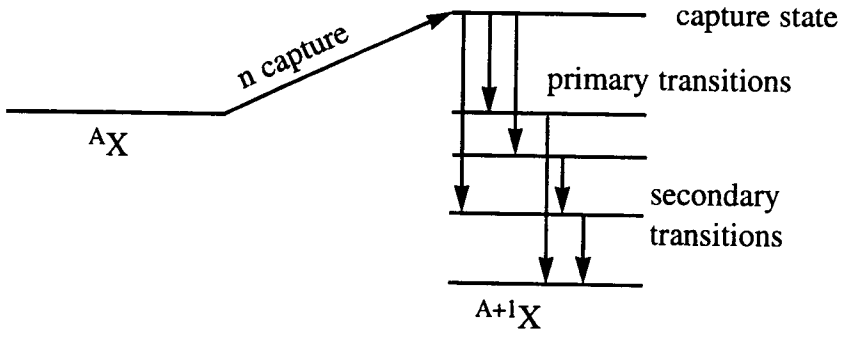

Figure 1. Schematic of (n,γ) process and γ-ray cascade.

Among its uses, neutron capture helps to decrease the number of slow neutrons in a particle beam that has a wide distribution of velocities, to verify neutron binding energies, to explain the abundance of isotopes in stellar nucleosynthesis [Cla68, Ejn98], and to examine the properties of the excited states of the nuclei involved. Neutron capture spectra also have been applied in in biomedicine, environmental studies, archeology, and the analysis of reactor materials and fuels [Chr84].

I.1 The neutron capture cross section.

The probability that a nucleus will capture a neutron depends primarily on the energy of the incident neutron (E_n), the type of target nucleus and its energy levels, the difference in rest-mass energies between the initial and final nuclides, and how long the neutron is in the vicinity of the target nucleus [All84]. An isotope's neutron capture cross section (σ_c) is an indication of how susceptible the isotope is to neutron capture and represents the probability that a target nucleus will capture the neutron. The cross section also is an indication of the effective size of the target nucleus and thus has the units of area (cm^2 or $b = 10^{-24}\ cm^2$). Neutron capture has been observed over a wide range of energies up to ~14 MeV. Figure 2, adapted from [Poe84], shows how σ_c varies with E_n for medium- and heavy-mass target nuclei.

For E_n less than 1 eV, σ_c has a strong $E_n^{-1/2}$ (or v^{-1}) dependence and is relatively large. The σ_c of some isotopes vary from this $E_n^{-1/2}$ dependence, especially if the neutron binding energy is close to the bound-energy levels in the target nuclei or if the ^{A+1}X configuration is more or less preferable in terms of energy or stability than is the configuration of ^{A}X.

Figure 2 also indicates that low-energy neutrons are, in general, more likely to be absorbed than are high-energy neutrons. Low-velocity (low E_n) neutrons spend more time in the neighborhood of the target nucleus than do high-velocity neutrons. Thus a slow neutron spends more time within range of the nuclear force, increasing its probability for capture. The E_n region between 10^{-8} and 10^{-6} MeV represents the thermal energy distribution of neutron velocities at temperatures of 300 K; that is, the incident particles have an average energy of $3kT/2$

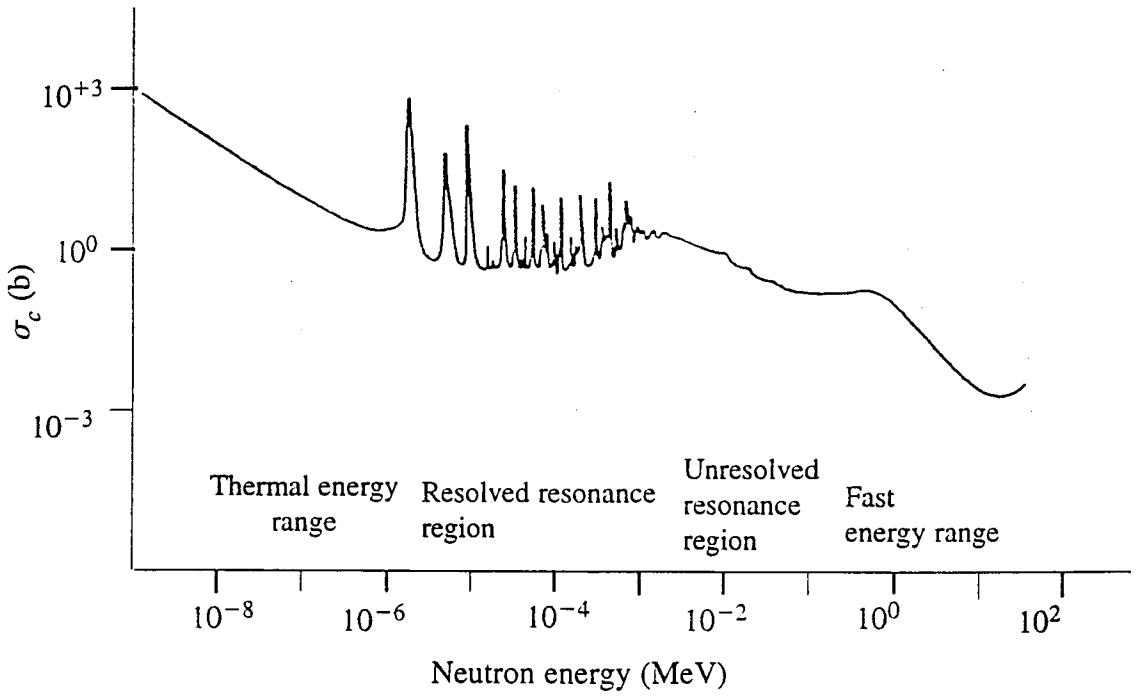

Figure 2. Variation of σ_c with neutron energy. (adapted from [Poe84])

(~0.039 eV for T = 300 K) where k is Boltzmann's constant and T is the absolute temperature [Cur59]. When reactor neutrons come to thermal equilibrium with a room-temperature moderator, they are referred to as *thermal* neutrons.

I.2 Challenges with radioactive targets.

Extensive studies have been conducted that have determined the σ_c of many stable isotopes [Mug81]. However, relatively little research has been done to determine the σ_c of radioactive targets. The capture cross section of a stable isotope target may be easier to measure than a radioactive isotope target because a radioactive isotope, by definition, undergoes radioactive decay. Thus the number of target sites available for capture is always decreasing in accordance with the material's half life ($t_{1/2}$). (The extent of this problem, of course, depends on the length of $t_{1/2}$ in comparison with the duration of the experiment.) Also, a 1-g sample of a stable isotope typically contains approximately 10^{23} nuclei available for particle capture. In contrast, a moderately sized radioactive sample normally contains between 10^{13} and 10^{14} available sites. Furthermore, commercially available radioactive material often contains impurities that can also capture the incident particles, become radioactive, and emit γ rays. These impurities can be present in the container used in the irradiation, the solvent (for sources in solution), or any analytical tool used to handle the material. The sample also can contain "carrier" isotopes, stable nuclei of the same element that are added in processing by the supplier to facilitate the extraction of the radioactive sample. Finally, radioactive sources often are available only in solution (HCl or NaOH), which can change phase during irradiation (e.g., undergo evaporation or crystallization), leading to the need for careful handling and redissolving, which may not be required for stable isotopes in solid form. This is especially complicated if the source is prone to react with the solvent (e.g., a hydrophilic material).

I.3 Activation method for finding σ_c.

If the capture of a neutron results in a radioactive ^{A+1}X nucleus and if the target material can be obtained with few impurities, then a simple irradiation-and-count experiment can be used to find σ_c. This is known as the activation or direct-measurement technique. About one-third of stable isotopes become radioactive after neutron capture [Poe84]. Similarly, many radioactive nuclei become stable after capturing a neutron and, therefore, would be unsuitable for measurement by this method. The major limitations of using the activation method when working with radioactive targets are as follows:

- The ^{A}X target nucleus must have a sufficiently long $t_{1/2}$ such that most of the nuclei do not decay during the experimentation time.
- There must be at least one transition that can be detected (i.e, the parent nucleus must not decay directly to the ground state). Although one energy peak in the spectrum is all that is needed do perform the measurement, there should be enough peaks in the spectrum so that the presence of ^{A+1}X can be positively identified.
- The ^{A+1}X isotope must have a $t_{1/2}$ short enough to permit its decay to be measured in a reasonable amount of time (thus, it cannot be stable). But the $t_{1/2}$ also must be long enough such that the ^{A+1}X isotope that is created does not decay too quickly.
- There may be limitations in the changes in spin between the ^{A}X decaying state and ^{A+1}X capture state. Low-velocity particles can transfer only a small amount of angular momentum to the target nucleus. Thus, there is a low probably that a slow, spin-1/2 neutron can be captured under any transaction that requires greater than an f-wave capture.

I.4 Other methods for finding σ_c.

The absorption and transmutation method involves finding σ_c by calculating the difference between the total cross section and the elastic scattering cross section. This is particularly useful in cases for which elastic scattering and neutron capture are the only reactions that occur below the first threshold for inelastic scattering. The total cross section can be determined by

using precise transmission techniques. Because the intensity of a beam though a material is related to $e^{-nx\sigma}$ (where x is the thickness of the material and n is the number of atoms per unit volume of the material) and because the scattering cross section is only a small fraction of the total cross section, this method typically leads to an uncertainty in the σ_c value that is smaller than the uncertainty in σ_c using a direct measurement technique. Although this method most likely could be used with radioactive samples, the technique requires that sensitive neutron detectors be positioned directly in front of the sample and neutron beam. This configuration was not possible at the facilities used for thermal activation for these experiments.

The spherical shell transmission method to determine σ_c has been described by Schmitt and Cook [Sch60]. In this technique, a spherical shell of the sample material is positioned between a neutron source and the neutron detectors. Comparing the known emission of the neutron source to the count of the neutron detectors provides a means of determining the absorption of the sampling material. In their experiment, Schmitt and Cook calculated the absolute neutron absorption cross section (the cross section for all processes in which a neutron is removed). In the keV range, this is equal to σ_c. The spherical shell transmission method has the advantage in that absolute detection efficiencies are obtained directly from the neutron transmission measurements. However, the disadvantage is that relatively thick samples are needed, thus increasing the probability for self resonances (resonances within the sample). Currently, sufficient amounts of radioactive sources for configuration into thick samples are difficult, if not impossible, to obtain, so the technique remains limited to mainly stable isotopes.

Another method is prompt γ ray activation analysis (now referred to as prompt γ ray analysis or PGA). This method involves measuring the γ ray emitted directly from the capture state while the source is being irradiated. PGA first was used to analyze samples of simple composition. In 1979, however, Failey et al. showed that PGA could be used to analyze complex samples [Fai79]. The most important advantage to this method is that the measurement technique is purely instrumental and no analytical manipulation of the sample is necessary.

Thus, it is often the method of choice for archeological and biosensitive samples . However, an important disadvantage is that the PGA method is insensitive to oxygen [Chr84]. In many samples, oxides account for as much as 97% of the total mass and so the oxidation states must be assumed. Also, because PGA is based on the analysis of γ rays from the primary transition de-excitation of the ^{A+1}X nucleus, the data must be gathered in a very short period of time. In order to properly identify the γ rays from the sample, the data must be compared to irradiated, pure-element standards. Currently, the commercial availability of pure standards of radioactive isotopes is very limited, so the use of PGA to measure the σ_c of radioactive isotopes is impractical.

Other methods, which are not discussed in detail here, include measurement of the sample's "danger coefficient," the pile-oscillator technique, and the use of a pulsed neutron field [Poe84]. Compilations of the thermal neutron capture cross sections of various isotopes and the technique used to measure them are provided in [Mug81].

II. THEORY AND DEFINITIONS

II.1 Exponential decay.

Any experiment in which a radioactive source is used must include the exponential decay equation:

$$a(t) = a_0 \, e^{-\lambda t} \tag{1}$$

where a is the activity and λ is the decay constant defined as $\lambda = (\ln 2)/t_{1/2}$. This equation is used to determine the radioactivity at a specific time t or how much activity remains after an elapsed time Δt. If the the activity is counted during a time interval Δt, the amount of activity must be corrected by a decay factor $f = e^{-\lambda \Delta t}$ because the number of nuclei decreases during the interval Δt. If $t_{1/2}$ is large compared with Δt, most of the isotope will still be present during Δt, thus the activity is approximately constant during this interval and $f \sim 1$. In the following experiments, $f \sim 1$ for both ^{148}Gd and ^{68}Ge. If $t_{1/2}$ of the ^{A}X target isotope is large compared with the total time of irradiation, the number of nuclei available for capture (N) also is approximately constant.

Counting the activity over a time interval Δt from t_1 to t_2 also introduces a counting factor, arising from the integral of the activity over Δt

$$\text{Counts} = \int_{t_1}^{t_2} a_0 \, e^{-\lambda t} dt = a_0 e^{-\lambda t_1} \, \frac{(1 - e^{-\lambda \Delta t})}{\lambda} \tag{2}$$

Dividing both sides by Δt shows that the counting rate in this interval is the activity at the start of the interval, $a_0 e^{-\lambda t_1}$, corrected by a counting factor:

$$\text{counting factor} = \frac{(1 - e^{-\lambda \Delta t})}{\lambda \Delta t} \tag{3}$$

That is, the measured counting rate in any time interval (counts/Δt) must be corrected by the counting factor to determine the activity at the beginning of the time interval.

II.2 Flux.

The number of incident particles passing through a unit of cross sectional area of a beam per second is known as the beam's flux (ϕ) and is on the order of 10^{13} for thermal neutrons from the OSU reactor. The flux on a target can be experimentally determined by placing an isotope with a well-known $t_{1/2}$ and σ_c in the target area along with the ^{A}X sample whose cross section is to be measured. An Fe sample was used as a flux monitor in these experiments.

II.3 Rate of ^{A+1}X nuclei creation.

The rate at which the ^{A+1}X nuclei are created (R) can be expressed in terms of the number of ^{A}X nuclei that are available for capture (N), ϕ, and σ_c: $R = (\phi)\,(\sigma_c)\,(N)$. But if the ^{A+1}X also is radioactive, it decays according to Equation 1 and the number of ^{A+1}X nuclei then decreases as well. The change in the number of ^{A+1}X nuclei is $dN = Rdt - \lambda(Ndt)$, for which the solution is $N(t) = (R/\lambda)\,(1 - e^{-\lambda t})$. Because $a = \lambda N$, the activity of the ^{A+1}X nucleus at any time while the sample is in the reactor is

$$a = R\,(1 - e^{-\lambda t}) \tag{4}$$

If the bombardment time (t_b) is much shorter than the $t_{1/2}$ of the ^{A+1}X isotope, then the exponential can be expanded and only the linear term can be kept so that $a(t) = R\lambda t$. This corresponds to a linear growth in activity. However, if the irradiation time is much longer than the $t_{1/2}$ of the ^{A+1}X isotope, the activity reaches a maximum at which point there are almost as many new nuclei being created as there are decaying, and $a = R$. This is the referred to as the "secular equilibrium point."

II.4 Equation for σ_c.

The equation for neutron capture cross section follows from Equation 4

$$\sigma_c = \frac{a_{EOB}}{\phi\, N\,(1 - e^{-\lambda t_b})} \tag{5}$$

where a_{EOB} is the activity of the ^{A+1}X isotope at the end of bombardment (EOB), N is the number of ^{A}X irradiated, t_b is the bombardment time, ϕ is the neutron flux in units of $(cm^2\ s)^{-1}$, and the λ is the decay constant of the ^{A+1}X isotope.

II.4 Detector efficiency.

The ratio of the number of radiations of a particular energy that are detected to how many are actually emitted is known as the detector's efficiency (ϵ). The detector's efficiency includes the solid-angle factor that determines the fraction of the emitted radiation that actually strikes the detector; thus the efficiency of a detector also depends on the source-to-detector distance and is proportional to $(\text{distance})^{-2}$. The source must be close enough to get a statistically useful counting rate, but not too close that the dead time (the time during which the system is processing the data and is not counting) prevents many of the particles from being counted. Determining the efficiency of the detector requires that a calibration standard be used. A calibration standard for these experiments is a radioactive source of known and validated activity. If the activity of this standard was measured at some past point in time, its current activity can be calculated by Equation 1. The efficiency at a particular energy is determined by peak area, live time (LT), activity a of the calibration source at the present time, and the γ ray's branching ratio $b(E)$

$$\epsilon = \frac{\text{Peak area}/LT}{a\,b\,(E)} \tag{6}$$

III. EXPERIMENTAL DETAILS

III.1 Experimental procedure and choice of target nuclei.

Gamma rays emitted from a radioactive source carry energies specific to that source. When the source is placed in front of a detector, the number of γ rays with each energy can be counted. If the counts are then plotted against the energy during a period of time, a spectrum showing the intensity of each γ ray is obtained. The γ-ray peaks may be difficult to observe depending on the resolution of the analyzer, impurities in the source, efficiency of the detector, and peaks resulting from any competing reactions such as (n,p) or Compton scattering. Integrating the net or gross area under the peaks (refer to section "Software and method of measurement") and dividing by *LT* gives a rough counting rate. Special attention must be paid to the method in which the peak's statistics, such as its net area, are found, especially when defining the region that constitutes the peak as opposed to a region that consists of only the background. This presents a problem if two or more energies are too close to resolve, resulting in at least double peaks (see ^{148}Gd experiment 346-keV data). However, if the peak is strong, well-resolved, and sits in a region with a relatively flat background, its intensity and decay can be used to monitor the activity and decay of the entire sample. Of course, each γ emission is only a portion of the total possible γ rays that could be emitted. The fraction of the total γ rays corresponding to the intensity of each individual γ ray is its branching ratio.

Stocks of high-purity ^{68}Ge and ^{148}Gd were available, met the conditions of the proposed experimentation method, and their σ_c values for had not been measured previously. Figure 3 shows the partial decay schemes of ^{68}Ge and ^{69}Ge. Figure 4 shows the partial decay schemes of ^{148}Gd and ^{149}Gd (adapted from [Fir96]).

^{68}Ge has a $t_{1/2}$ of 271 days and ^{69}Ge has a $t_{1/2}$ of 39 h. If the experiment is carried out over a period of about 7 days, the number of ^{68}Ge nuclei remains relatively constant while the γ rays of ^{69}Ge can be observed. Figures 5 outlines the experimental procedure used for the ^{68}Ge experiment. ^{68}Ge decays only by electron capture and emits no γ rays. However, the

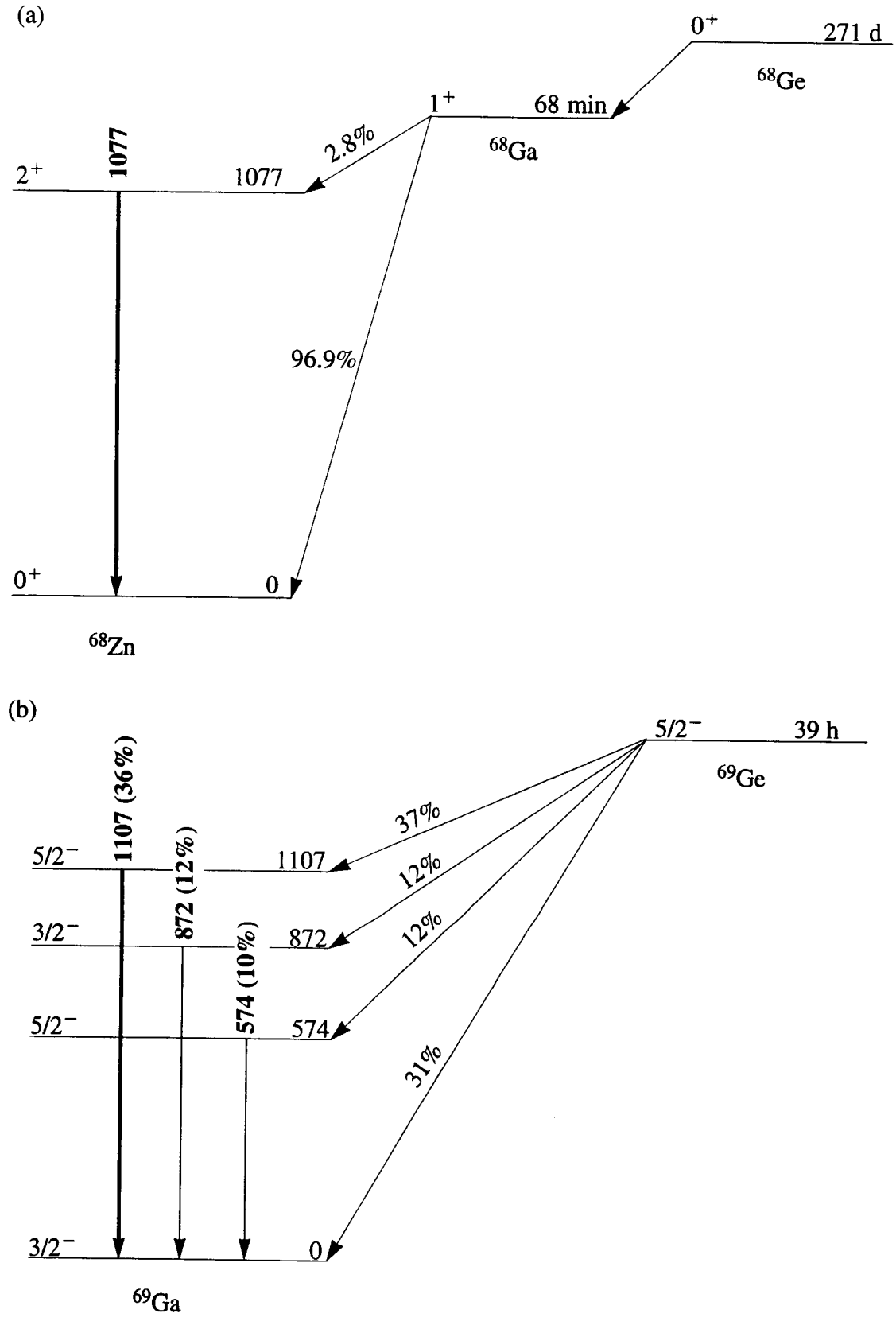

Figure 3. Partial decay schemes of (a) ^{68}Ge and (b) ^{69}Ge.

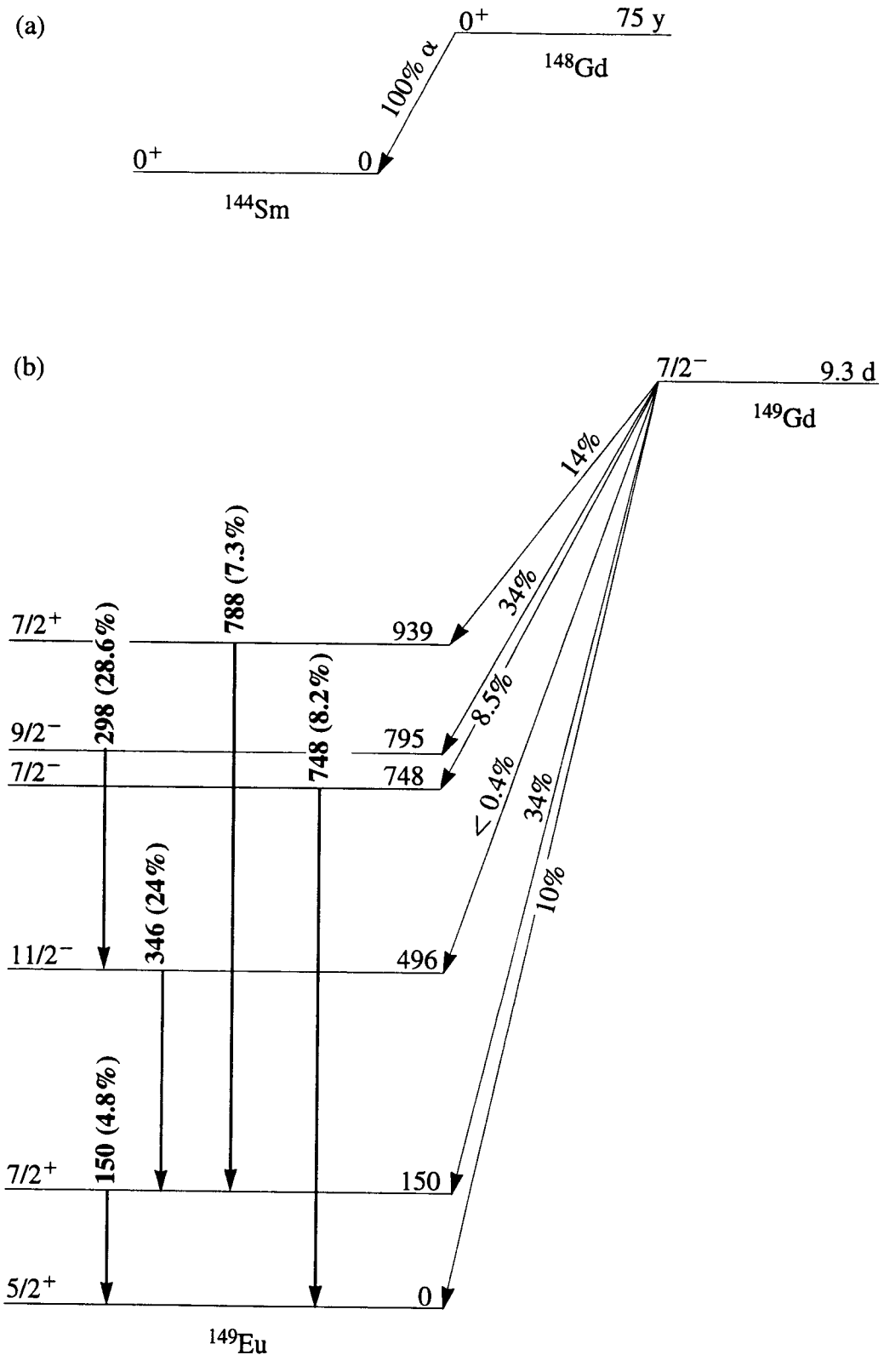

Figure 4. Partial decay schemes of (a) ^{148}Gd and (b) ^{149}Gd.

subsequent decay of ^{68}Ga emits a 1077-keV γ ray, which can be used as a monitor for ^{68}Ge. The best peak to analyze for the presence of ^{69}Ge is at the 1107-keV energy with a $b(E_\gamma)$ = 36%. Monitoring the decay of the 1107-keV peak can be used to determine the activity of ^{69}Ge. The flux will be determined by the irradiated Fe sample. Using these data in Equation 5 provides a value for σ_c.

^{148}Gd emits only α rays and ^{149}Gd emits mostly γ rays. Figure 6 outlines the procedure for this experiment. An irradiated ^{148}Gd sample's α-particle activity indicates how many ^{148}Gd nuclei are present (N^{148}), and the amount of γ-ray activity will indicate how much ^{149}Gd is present in the sample. The flux can be determined in the same manner as for the ^{68}Ge experiment. Using these data in Equation 5, σ_c can be determined.

III.2 Equipment.

Each radioactive target was neutron irradiated in the thermal column of the Oregon State University 1-MW TRIGA reactor. The γ-ray spectra after irradiation were observed using an Ortec high-purity Ge detector. The detector was enclosed in low-activity Pb housing. The detector was connected to an Ortec 572 amplifier, which was connected to a PC for data acquisition.

The α-particle spectra of an extracted sample of the irradiated ^{148}Gd was observed using a bell jar, vacuum pump, and a silicon detector connected to a PC for data acquisition.

III.3 Software and method of measurement.

Data were obtained using PC-compatible Maestro software (EG&G Ortec, Inc., 1992) to provide multichannel analyzer emulation. The software program processes the data gathered by a multichannel analyzer and displays the number of counts (on a vertical scale) per energy channel (on a horizontal scale). The horizontal scale is calibrated to show the energy in keV.

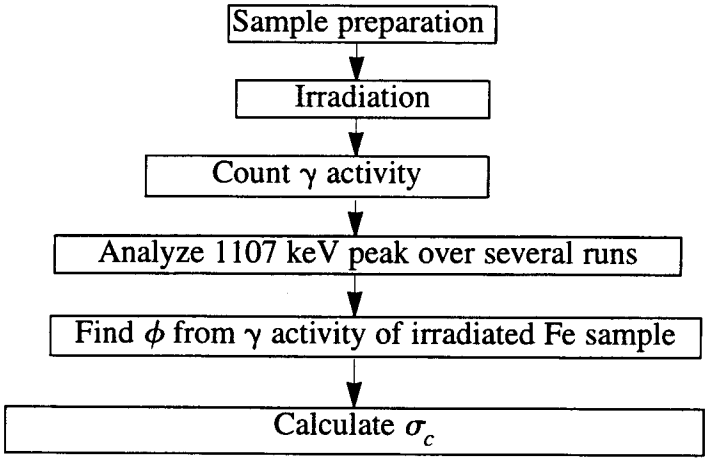

Figure 5. Procedure for ^{68}Ge experiment.

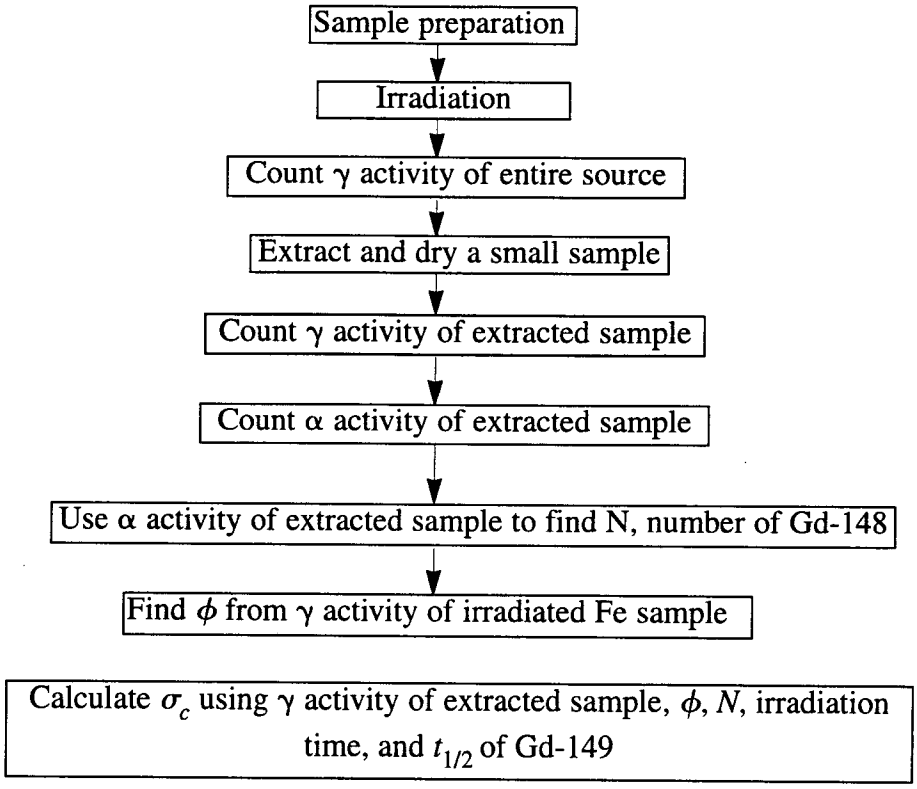

Figure 6. Procedure for ^{148}Gd experiment.

To analyze a peak, the user must select a region of interest (ROI) of a specific width, symmetric about the maximum point of the peak. After an ROI is defined, the program then provides both the gross area and the net area. The gross area is simply a sum of all the counts for each channel within the ROI, including the background. Gross areas were used to analyze the spectra of three α-particle emitting calibration sources in the ^{148}Gd experiment. In the ^{68}Ge experiments, gross areas also were used to calculate the number of counts in the very low-intensity peaks of interest. In cases for which the spectrum has visible peaks against a background, the net area option provides the number of counts in the peak as well as an uncertainty. The program calculates the net area by taking two points, one that is three channels from the left side of the ROI and the other that is three channels from the right side, and defining the peak as everything above the line connecting the two points. Most of the calculations involved net area counts.

III.4 First ^{68}Ge experiment.

Sample preparation and irradiation. A 51 μCi stock sample of ^{68}Ge was obtained from Los Alamos National Laboratory with the following specifications:

- form: Ge (IV) in <1 M HCl
- activity: concentration >10 mCi/mL, theoretical sp. act = 6638 Ci/g Ge
- chemical impurities <1000 ppm
- radiopurity > 99%
- source: spallation by protons in natural rubidium bromide and molybdenum targets

The sample was prepared in a germanium tetrachloride solution, $GeCl_4$. The ^{68}Ge sample was placed in a 2/5-dram polyethylene vial. A 69-mg sample of Fe that would be used as a flux calibration source was placed in a second vial, and both vials were placed in an outer 2-dram polyethylene vial. Irradiation was performed in the OSU reactor from 08:28 to 16:28 on February 4 1998 (Table 1).

Table 1. ^{68}Ge experiments timeline.

Feb. 4 1998	08:28	Start irradiation
	16:28	End irradiation (EOB)
Feb. 5		Sample preparation and test runs
	10:25	^{60}Co calibration at 10 cm for LT = 301.14 s
	10:48	^{152}Eu calibration at 10 cm for LT = 400.54 s
	16:27	Start Gd-a runs at 10 cm for LT ~2200 s
Feb 6		Gd-a runs stopped after 17 runs
	09:45	Start Ge-18a run for 1 h (end at 10.45)
	11:23	Start Ge-b 1-h (real time) runs at 10-cm
Dec. 9		Sample preparation for second ^{68}Ge experiment
Dec. 15		8-h irradiation of second ^{68}Ge source
Dec. 16		8-h irradiation of second ^{68}Ge source
Dec. 17		8-h irradiation of second ^{68}Ge source
		^{152}Eu calibration run 2
		Count ^{68}Ge source from first experiment
Dec. 18		Extract sample, conduct test runs
		^{152}Eu calibration runs 4 and 5
	10:19	Start Ge-c runs, real time = 3600 s
Dec. 19	18:19	Ge-c runs are accidentally stopped after 32 runs
Dec. 21	08:45	^{152}Eu calibration run 6
	09:55	^{152}Eu calibration run 7
	11:10	Irradiated Fe count started

Gamma detector efficiency. A ^{60}Co calibration source (a = 0.884 μCi on March 1, 1987, Isotopes Products #173-13-17) was placed 10 cm from the Ge detector and counted for 301.14 s *LT* (real time = 304.20 s). A ^{152}Eu calibration source (a = 1.133 μCi on Feb. 1, 1985, Isotopes Products source #12624-3) also was placed 10 cm from the detector and counted for *LT* = 400.54 s (real time = 411.94 s) starting at 10:48. The activities and efficiencies of the γ rays of the ^{152}Eu and ^{60}Co calibration sources are shown in Table 2. The relationship between energy and efficiency is shown in Figure 7.

Gamma-ray activity data collection. After irradiation, the vials were uncapped and rinsed with distilled water. The solution was placed in a clean vial. Test runs were conducted on the irradiated Ge source, the vials, and the Fe sample. The outer vial did not appear to contain ^{69}Ge, but it did show a strong presence of an impurity at approximately 1368 keV, identified as ^{24}Na. Most of the irradiated ^{68}Ge appeared to have remained in the inner vial. This was apparent by taking quick calculations of the activity of the test runs. For example, the first calculation showed that only about 8.8 μCi ($a = 3.26 \times 10^5$/s) were extracted from the vial. The irradiated 2/5-dram vial was placed in front of the γ detector and counted. The resultant spectrum showed that ^{68}Ge activity was still present. Additional HCl and water was added and allowed to sit in the vial for approximately an hour. The solution was then added to the previous counting solution and counted at 10 cm from the detector. This run showed that the ^{68}Ge activity in the sample was 10.7 μCi ($a = 3.96 \times 10^5$/s).

A series of 1-h runs (labeled as "Ge68-a") was started at 16:27 on February 5, 1998. After 17 runs, the program was stopped, and another 1-h run (labeled "Ge-18a") was begun at 09:45 on February 6. A second series of 1-h runs (labeled as "Ge68-b") was begun 11:23 on February 6. A program was set to gather 99 1-h runs (i.e., 99 spectra). The first nine spectra of the Ge68-a series (Ge68-01a to Ge68-09a) was summed as was the last nine spectra (Ge68-10a to Ge68-18a). Eleven sums, of nine spectra each, were also gathered for the Ge68-b series.

Table 2. Gamma detector efficiency data for first ^{68}Ge experiment.

True E (keV)*	**Exp. E (keV)****	**b(E_γ) (%)**	**Net area**	**ϵ (10^{-3})**
From ^{152}Eu source:				
121.78	121.55	28.4	21,114 ± 154	8.67
244.70	244.39	7.5	3824 ± 72	5.95
295.94	295.62	0.44	182 ± 24	4.83
344.28	343.97	26.6	11,254 ± 111	4.93
367.79	367.49	0.834	302 ± 26	4.22
411.11	410.61	2.23	712 ± 33	3.73
443.98	443.54	2.78	1011 ± 41	4.24
488.66	488.50	0.41	111 ± 19	3.16
564.02	563.51	0.47	97 ± 21	2.40
778.90	778.34	12.96	2504 ± 56	2.25
867.39	866.94	4.15	825 ± 36	2.32
964.13	963.65	14.33	2395 ± 56	1.95
1112.12	1111.84	13.54	2240 ± 53	1.93
1408.01	1407.69	20.87	2727 ± 57	1.52
From ^{60}Co source:				
1173.21	1172.73	100	4030 ± 68	1.74
1332.47	1331.90	100	3758 ± 65	1.62

**True E is the energy as shown in reference [Fir96].
*Exp. E is the energy of the peak shown in the spectra

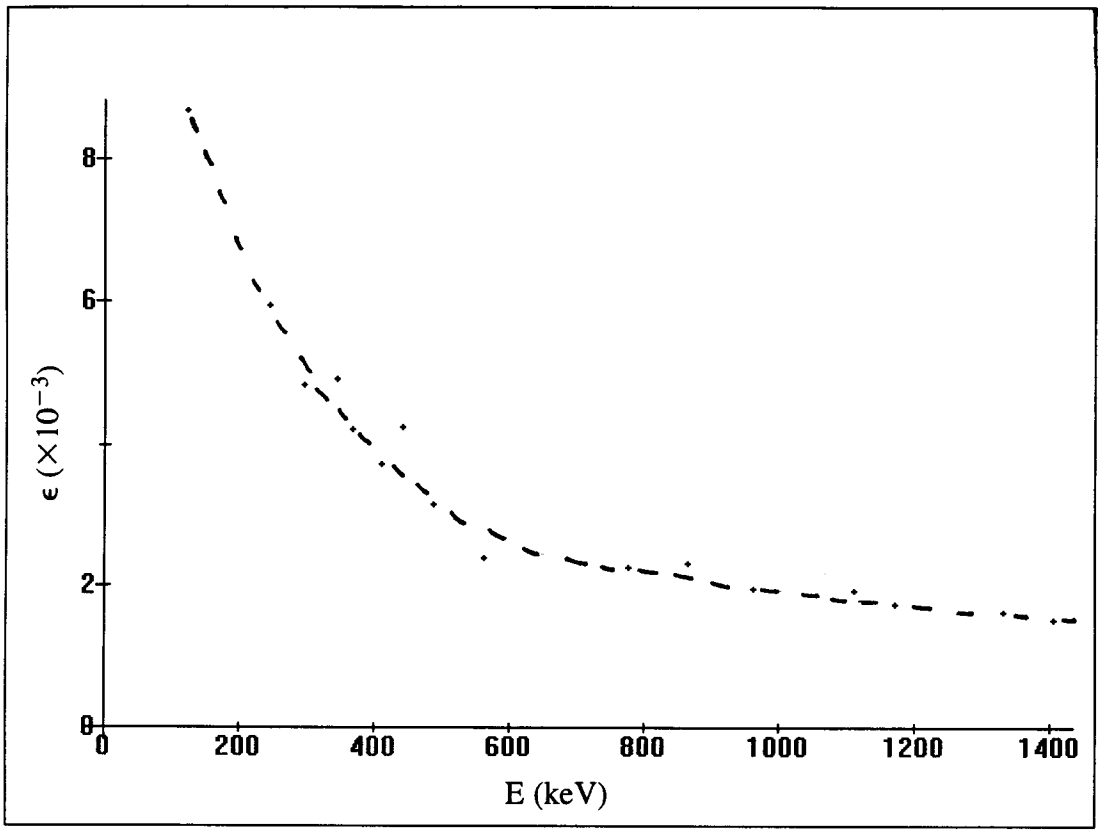

Figure 7. Gamma detector efficiency for first ^{68}Ge experiment.

III.5 Second ^{68}Ge experiment.

Sample preparation and irradiation. In hopes of gaining an increase in intensity of the ^{69}Ge peaks and a decrease in the intensity of the 1368-keV line from the ^{24}Na impurity, a second ^{68}Ge experiment was planned for an irradiation of 24 h (three 8-h irradiations over three days). On December 9, 1998, a second ^{68}Ge source was received in a 0.4-dram vial with the same specifications as the first stock source. The $GeCl_4$ liquid was extracted using a long, thin pipette with a diameter of ~2 mm. The liquid was then transferred to a quartz vial and topped with a rubber stopper. The use of a quartz vial (as opposed to a polyethylene vial used in the first ^{68}Ge experiment) was required by the radiation facility. The dimensions of the liquid in the vial were about 0.25×5 in^2 (diameter $\times$ length). The tube was then heated and sealed to a length of about 3 in. A 71-mg Fe sample to be used as a flux monitor was sealed in a similar tube. Approximately 85% (45 μCi) of the original sample was estimated to be extracted from the original stock ^{68}Ge container. The ^{68}Ge liquid in the quartz vial was then irradiated over three days, December 15–17, 1998, for 8 h each day (Table 1).

Gamma detector efficiency. Four runs of a known ^{152}Eu source (a = 1.133 μCi on February 1, 1985, Isotope Products #16500) were used to find the efficiency of the γ detectors at 3 cm. To reduce detector dead time, two of the runs included the use of 1/8-in. thick Pb and Cu plates placed between the source and the detector. On December 18, 1998, runs labeled "Eu-cal4" (without the absorbing plates) and "Eu-cal5" (with the absorbing plates) were completed with *LT*s of 950 s and 976 s, respectively (Table 3). After the ^{68}Ge γ spectra were recorded, a second set of ^{152}Eu calibration runs was gathered, with and without absorbing plates. These spectra were labeled "Eu-cal6" (with absorbers) and "Eu-cal7" (without absorbers). Figure 8 shows the relationship between efficiency and energy for these four calibration runs.

Table 3. Gamma detector efficiency data for second ^{68}Ge experiment.

True E (keV)	Exp. E (keV)	b(E_γ) (%)	Net areas and efficiencies							
			Eu-cal4*	ϵ(E)	Eu-cal 5**	ϵ(E)	Eu-cal6**	ϵ(E)	Eu-cal7*	ϵ(E)
121.78	121.95	28.4	104,579±339	.0189					372,355 ± 641	.0178
244.70	244.65	7.5	20,836±159	.0143	2060±69	.00137	7355±130	.00136	73611±299	.0133
344.28	344.37	26.6	54,231±246	.0105	17,381±14	.00327	63,058±270	.00330	197,211±462	.0100
411.11	411.10	2.23	3939±76	.0091	1811±57	.00406	5744±108	.00358	13,138±141	.00798
443.98	444.08	2.78	4891±84	.0090	2314±63	.00416	8626±119	.00431	17,266±155	.00842
778.90	779.22	12.96	13,100±129	.0052	9114 ±108	.00352	33,257±206	.00356	46,477±241	.00486
867.39	867.69	4.15	3654±78	.0045	2813±69	.00339	10,046±130	.00336	13,300±147	.00434
964.13	964.40	14.33	12,253±123	.0044	9323±107	.00325	32,689±205	.00317	42,029±234	.00397
1112.12	1112.35	13.54	10,337±119	.0039	8079±106	.00298	29,997±196	.00307	38,466±222	.00385
1408.01	1408.50	20.87	13,669±121	.0034	11,140±108	.00267	39,370±210	.00262	47,997 234	.00312
	Live time		**950 s**		**976 s**		**3514 s**		**3426 s**	

*Eu-cal4 and Eu-cal7 were run without the Pb and Cu absorbing plates.
**Eu-cal5 and Eu-cal6 were run with the Pb and Cu absorbing plates.

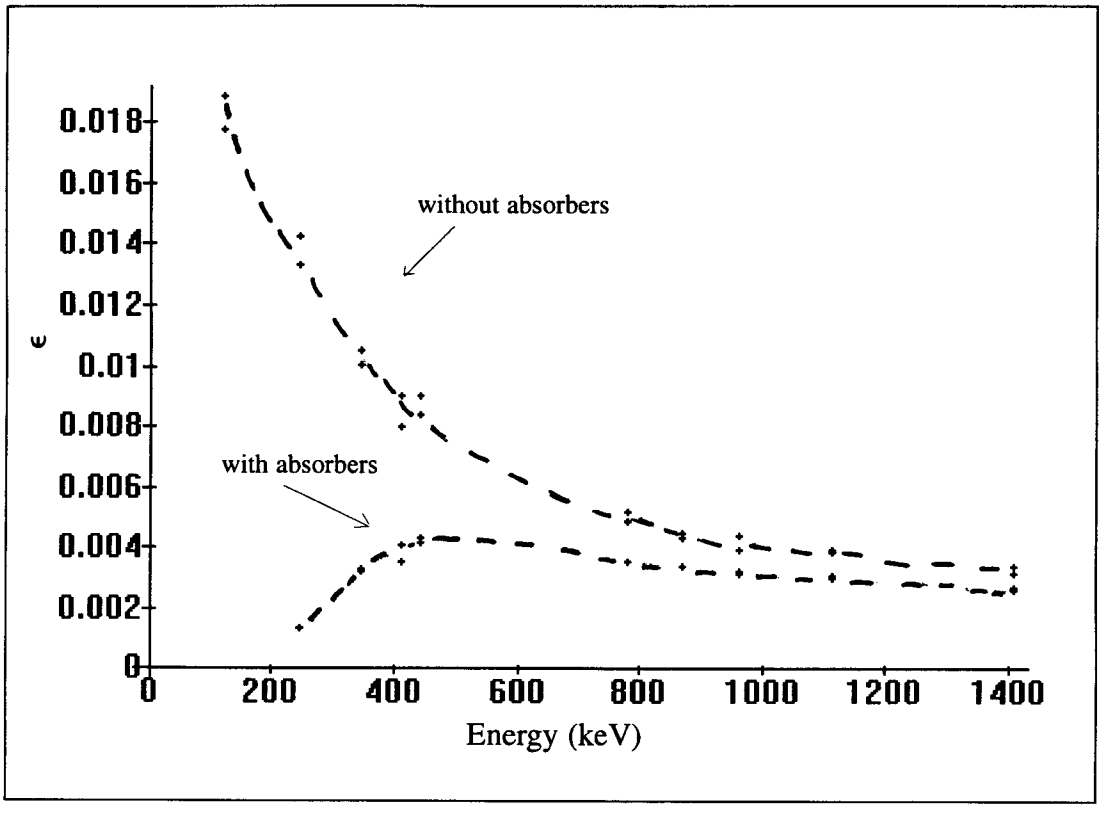

Figure 8. Gamma detector efficiency for second ^{68}Ge experiment.
(Data provided in Table 3.)

Gamma-ray activity data collection. On December 18, 1998, the irradiated ^{68}Ge sample was removed from the chamber. The quartz tube was placed in a 0.4-dram polyethylene vial and set in a Pb block. With a file, the top of the quartz vial was scarred. When attempting to snap off the upper portion of the vial, the vial exploded into small glass fragments. Much of the material was collected in the poly vial and most of the activity seemed to have been imbedded in the sides of the Pb block. The sides of the block were rinsed with distilled water and collected in a 2-dram polyethylene vial. The fragments were collected in a second vial. A count of this vial containing the fragments was conducted in front of a Ge detector. Minimal activity was seen, so the vial containing the solution of rinsed-off activity was used for data collection. The cause of the explosion is unknown. However, one possibility is that the three-day irradiation may have excessively heated the germanium tetrachloride solution, which is known to be "appreciably volatile at room temperatures" [Mer89].

At 10:19 on December 18, 1998, a series of 1-h (real time) runs was started (labeled "Gd-c) at 3-cm from the Ge detector. However, the experiment was stopped accidentally after only 32 runs. The data were summed into four 8-h blocks.

III.6 ^{148}Gd experiment.

Sample preparation and irradiation. A ^{148}Gd sample was obtained from Los Alamos National Laboratory with the following specifications:

- form: Gd (III) in 0.1 M HCl
- activity: concentration $>$ 1 μCi/mL, theoretical sp. act. = 32.4 Ci/g Gd
- chemical impurities $<$ 5000 ppm
- radiopurity $>$ 99.9%
- source: spallation by proton in natural tantalum targets

The ^{148}Gd stock sample was placed in a 2/5-dram polyethylene vial and capped. The vial was then enclosed in a 2-dram outer vial, and a 74-mg Fe sample was enclosed in a separate inner vial. The Fe sample again would be used to measure the neutron beam's flux. The

thermal column of the Oregon State University 1-MW TRIGA reactor provided an 8-h irradiation on 7 October, 1998. Table 4 shows the date and time for each important step in the experiment. Establishing a $t = 0$ reference point is important for comparing spectra taken at different times and for accurately calculating the activity after a known and well-defined Δt.

Gamma-detector efficiency. To find the efficiency of the γ detector, a ^{152}Eu calibration source was positioned at 12 cm from the detector during a LT = 5838.40 s at 13:35 on October 12, 1998. The activity of the ^{152}Eu source was 1.418 μCi on March 16, 1987, so by Equation 1 the activity at the time of measurement was a = 0.781 μCi. Table 5 shows the net areas for the γ transitions of ^{152}Eu. The true energies and branching ratios, $b(E_\gamma)$, were obtained from [Fir96], and the efficiencies were calculated using Equation 5. Figure 9 shows the efficiency versus energy plot.

Gamma activity data collection. After irradiation, the vials were removed from the reactor. Neither of the vials appeared to contain the liquid. The inner vial was opened and rinsed with doubly distilled water. The cap of the inner vial also was rinsed. The water-rinsed sample was placed in a single polyethylene vial and positioned 16 cm in front of the γ detector. During a 600-s LT run the 149-, 298-, and 346-keV peaks were easily identifiable, indicating the presence of ^{149}Gd. The most prominent peak was at 298 keV. To ensure that a significant amount of ^{149}Gd had been rinsed off, the inner vial was placed in front of the detector at the 16-cm position. During a 600-s LT run, the net area of the 298-keV peak was nearly four times less than the area of the 298-keV peak shown in the count of the water-rinsed sample. Therefore, it was unnecessary to extract more activity from the inner vial. The activity of the outer vial was counted at the 25-cm position. During a 600-s LT run, the net area of the 298-keV peak was less than 10% of the area from the water-rinsed sample. Thus, we concluded that about 80% of the sample had been extracted and that extracting more activity from the outer vial was unnecessary.

Table 4. ^{148}Gd experiment timeline.

Oct. 7, 1998	08:30	Irradiate ^{148}Gd source and Fe sample
	16:30 (EOB, $t = 0$)	Stop irradiation. This is the $t = 0$ reference point.
Oct. 8		Test runs
	16:45	Placed irradiated Gd source at 16-cm position, start Gd-b runs
Oct.9	11:58 (SOM, $t = 43.47$ h)	Start Gd-b runs again at 12-cm position, real time 6000s
Oct. 12	13:25	Gd-b runs stopped after 44 1-h (real time) runs
	13:35	Start ^{152}Eu calibration run at 12-cm position,
Oct. 13	13:14	Start counting Fe sample at 12-cm position (real time 6000s, LT= 4906.98 s)
		Prepare first extracted sample to be used for α counts, and conduct test runs
Oct. 14		^{241}Am, ^{148}Gd α count runs
	13:30	Extracted 5 drops, α count, real time = 3601.20 s, LT = 3600 s
Oct. 15	08:50	^{230}Th α count run
	15:49 ($t = 191.32$)	Start Gd-c runs, γ counts of first extracted sample, real time = 7200 s at 12-cm position
Oct. 16	09:49	Stop Gd-c runs after 10 runs
Oct. 20		Extracted second sample
	15:07	Alpha count of second extracted sample, LT= 7200s,
	15:19 ($t = 310.82$ h)	Start Gd-d runs, γ counts of Gd source remaining after second extraction, at 12-cm position, real time = 6000 s
Oct. 21	06:19	Stop Gd-d runs after 10 runs
	11:43	New ^{152}Eu calibration spectrum at 12-cm position
	13:38 ($t = 333.14$ h)	Start Gd-e series runs, γ counts of second extracted sample at 12-cm position, real time = 6000 s

Table 5. Gamma detector efficiency data for ^{148}Gd experiment.

True E (keV)	Exp. E (keV)	b(E_γ)(%)	Net area	ϵ (10^{-3})
121.78	122.11	28.4	355,120 ±681	7.39
244.70	243.96	7.5	69,457±326	5.47
295.94	295.91	0.44	3166±110	4.25
344.28	344.19	26.6	187,433±474	4.16
367.79	367.67	0.834	6036±155	4.27
411.11	410.73	2.23	13,376±152	3.54
443.98	443.62	2.78	17,655±191	3.75
488	488.24	0.41	1972±83	2.84
564.02	563.66	0.47	1877±81	2.36
586.29	585.84	0.46	2104±126	2.70
688.68	688.14	0.835	3189±101	2.26
778.90	778.82	12.96	45,881±243	2.09
867.39	866.64	4.15	13,621±164	1.94
964.13	963.19	14.33	43,676±232	1.80
1112.12	1110.90	13.54	37,807±238	1.65
1212.95	1211.37	1.40	3511±90	1.48
1299.12	1297.75	1.6	3881±77	1.43
1408.01	1406.57	20.87	46,839±222	1.33

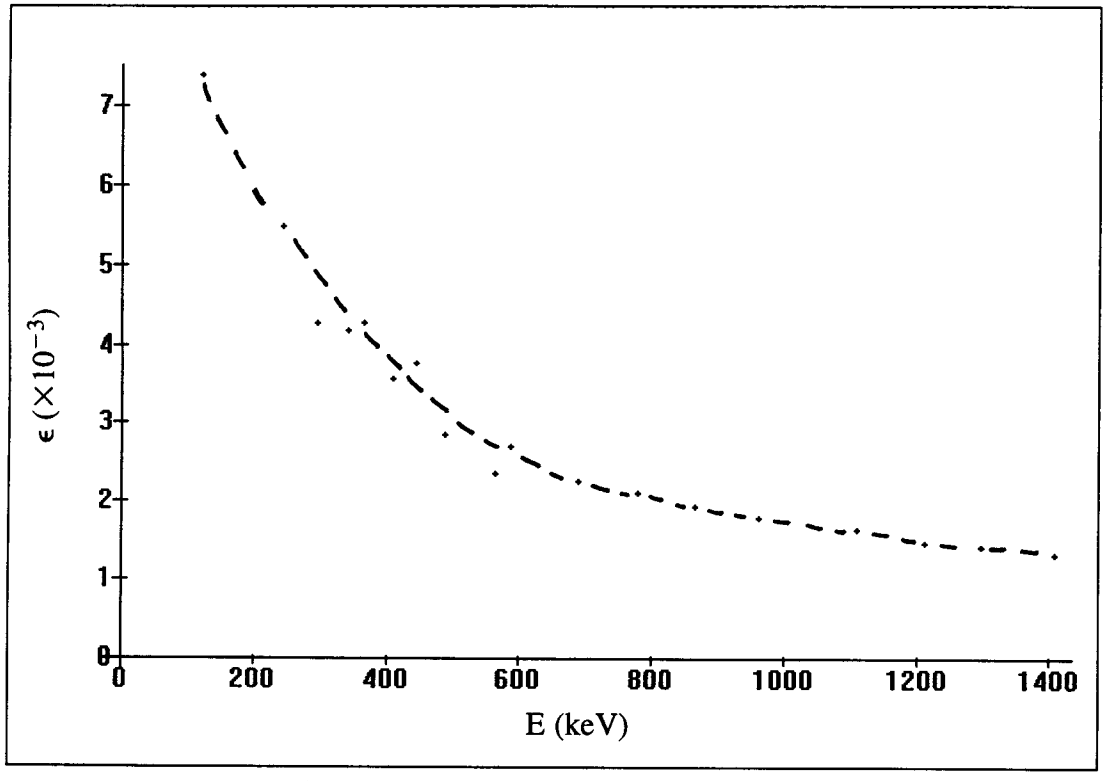

Figure 9. Gamma detector efficiency for ^{148}Gd experiment.

All of the spectra showed higher energy peaks at 411, 511, and 564 keV. A double peak appeared at 344 and 346 keV. The Maestro program was set to run 99 counts continuously, each with a *LT* of 1 h and with the liquid sample placed at 16 cm from the detector. However, because of a program error, the runs were started again 11:58 on October 9 at the 12-cm position. The spectra were labeled as "Gd-b" series files.

Alpha-particle activity data collection. A thin sheet of aluminum foil was glued onto a rubber ring. Approximately five drops were extracted from the liquid sample, placed onto the foil, and dried to evaporation under a heat lamp. After drying, the sample was placed on a platform and under a bell jar at approximately 4.8 cm from an α detector. A vacuum pump was used to ensure that no air was left in the jar. A typical α-particle spectrum from the ^{148}Gd source is shown in Figure 10. The spectrum shows only the 3.18 MeV peak from the ^{148}Gd and a small impurity peak at 5.25 MeV from ^{240}Pu, which had previously contaminated the silicon detector.

Alpha detector efficiency. To check the efficiency of the α detector, known calibrated sources of ^{241}Am, ^{230}Th, and ^{148}Gd were placed on the platform at 4.8 cm from the detector, and their α-particle spectra were recorded.

The ^{241}Am source ($t_{1/2}$ = 432.2 y) had a known activity of 0.1157 μCi on June 1, 1989. A 600-s *LT* run was started at 14:18 on October 14. The peak at the 5486 keV point had a gross count of 24,488 between an ROI width from 146 to 165. ^{241}Am has several α peaks between these two markers: 5486 (85%), 5443 (13%), 5338 (1.4%), 5544 (0.341%), and 5512 (0.2%) keV. The peaks at each of these energies were not fully resolved, thus their branching ratios were added (total ~100%) and used in the Equation 6.

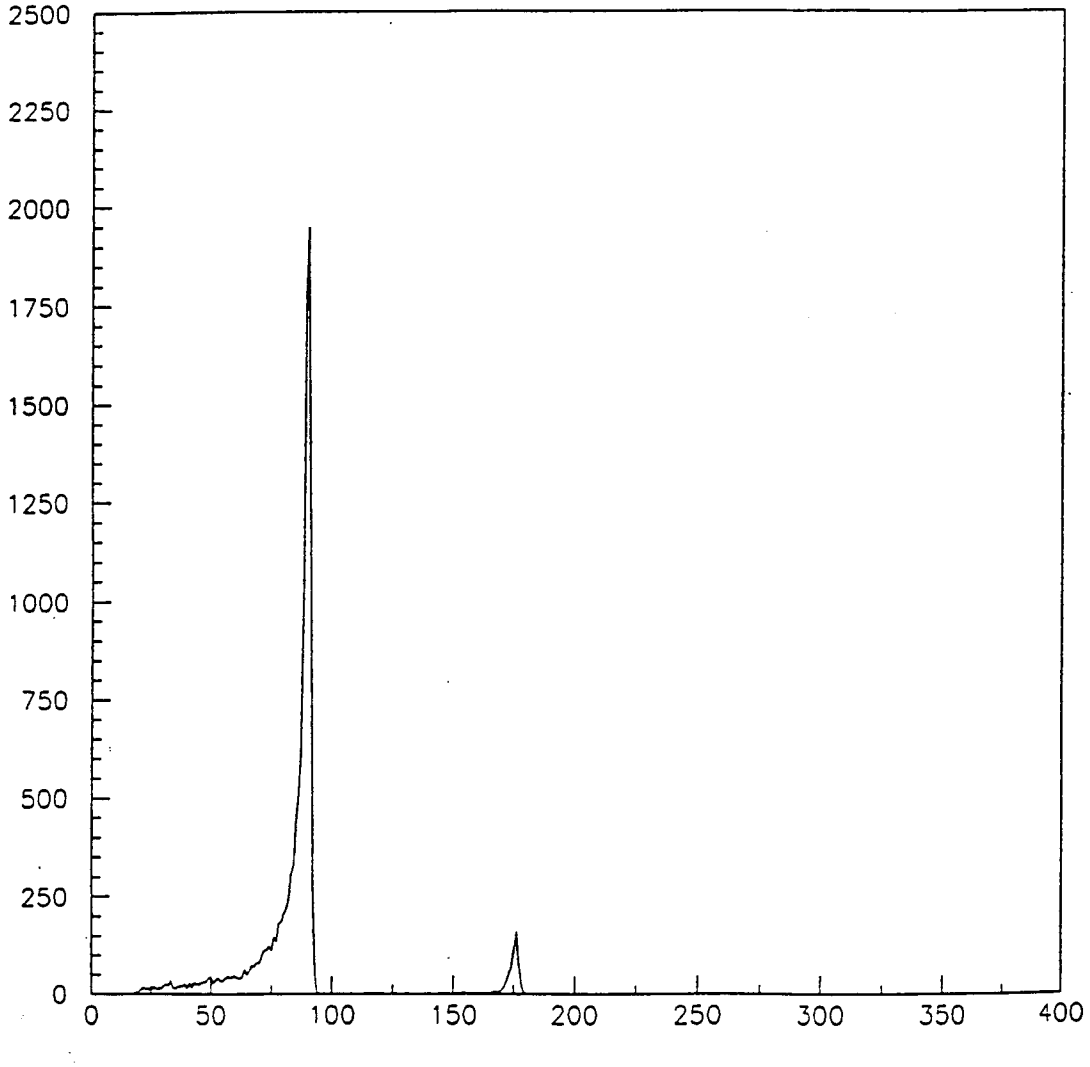

Figrure 10. Alpha-ray energy spectrum of irradiated ^{148}Gd.

Using Equation 1 the activity of the ^{241}Am source was calculated to be 0.114 μCi = 4.22×10^3/s. The efficiency of the α detector using the ^{241}Am source is

$$\epsilon_\alpha(^{241}\text{Am}) = \frac{24{,}488 \text{ counts} / 600 \text{ s}}{(4.22 \times 10^3/\text{s})(0.999)} = 9.68 \times 10^{-3} \quad (7)$$

The ^{230}Th source had a known activity of 4.72×10^{-3} μCi on June 1, 1989 and has a $t_{1/2}$ of 7.538×10^4 y, making the current activity $a = 1.75 \times 10^2$ /s by Equation 1. ^{230}Th emits two α-particles at energies 4688 (76.3%) and 4621 (23.4%) keV. During a 7200-s *LT* run, only one broad peak appeared with a gross area of 11,383. Because the peak included both the 4688 and 4621 keV regions, the ROI was set to cover both areas, and the sum of their branching ratios (total 99.7%) were used in Equation 6 to obtain

$$\epsilon_\alpha(^{230}\text{Th}) = \frac{11{,}383 \text{ counts} / 7200 \text{ s}}{(1.75 \times 10^2/\text{s})(0.997)} = 9.06 \times 10^{-3} \quad (8)$$

The ^{148}Gd calibration source had a known activity of 5.841×10^2 /s on August 13, 1979 and has a $t_{1/2}$ = 74.6 y, making the current activity $a = 4.888 \times 10^2$/s. It emits one α-particle with an energy of 3271 keV, and the ROI was set from channel 84 to channel 96 to cover this peak. During a 3600-s *LT* run, the α-particle energy had a gross area of 15,519 counts, making the α-detector efficiency calculation

$$\epsilon_\alpha(^{148}\text{Gd}) = \frac{15{,}519 \text{ counts} / 3600 \text{ s}}{(4.89 \times 10^2/\text{s})(1)} = 8.81 \times 10^{-3} \quad (9)$$

The average of these ε values, which are in good agreement with each other, is 9.18×10^{-3}. This value will be used for the efficiency of the α detector.

IV. RESULTS AND ANALYSIS

IV.1 First ^{68}Ge experiment.

A typical ^{68}Ge spectra is shown in Figure 11. Unfortunately, the strongest ^{69}Ge γ ray at 1107 keV (36%) was not clearly visible and was very close to an apparent ^{65}Zn impurity at 1115 keV. The challenge was to effectively analyze an 1107 keV peak by choosing an ROI that was wide enough to include all of the intensity of the 1107-keV "peak" without including too much of the background. If the ROI is too wide, the counts in the background will be attributed to the peak and the calculations will make the peak larger than it really is.

One way of finding a good width for the ROI is by looking at another peak near the 1107 keV region. The 1115- and 1260-keV peaks had all of their intensities fit within a 16-channel-wide ROI. Taking a 16-channel-wide ROI centered about the 1107-keV point allows for *two* 16-channel-wide ROIs to be taken for the background. One background ROI is taken above the 1107-keV region, and one is taken below. In other words, the ROI for the 1107-keV "peak" includes the peak plus the background. The *two* 16-channel-wide ROIs for the background makes the background region twice as wide as the peak region, reducing the amount of uncertainty, so that

$$\text{Area}_{\text{peak}} = (\text{Area}_{\text{peak + bkgr}} - 1/2\ \text{Area}_{\text{bkgr}}) \pm (\text{Area}_{\text{peak + bkgr}} + 1/4\ \text{Area}_{\text{bkgr}})^{1/2}$$

The last term is the uncertainty, and if the ROI for the background were as large as the ROI for the peak, then the sum in the square root would be larger.

^{69}Ge activity. The gross area of the peaks plus background as well as the gross area of the background was found for the ^{68}Ge-a and ^{68}Ge-b spectra sets (Table 6).

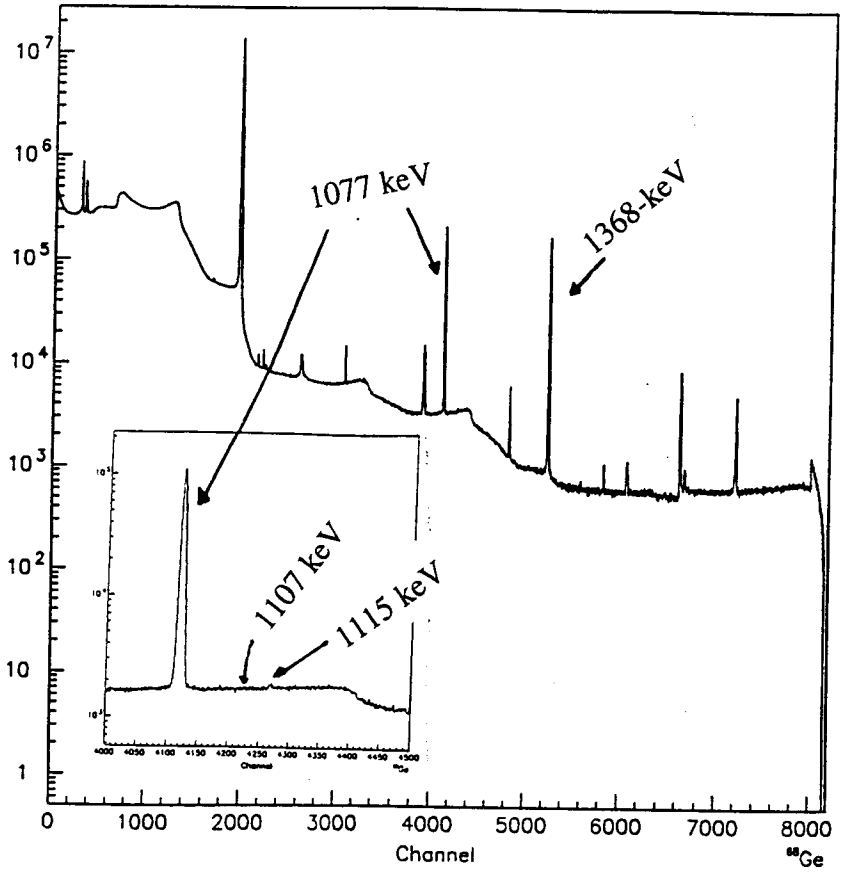

Figure 11. Gamma-ray energy spectrum of irradiated ^{68}Ge.

To find the correct counting rate, the peak area for each run was divided by the respective *LT* sum and corrected as shown in Equation 10.

$$\text{Counting rate} = \left(\frac{\text{Peak area}}{\text{LT}}\right)\left(\frac{1}{\text{counting factor}}\right)\left(\frac{1}{\text{decay factor}}\right)^{n-1} \tag{10}$$

where $n = 1$ for the first set of runs (1a–9a), $n = 2$ for the second set of runs (10a–18a), etc. For a 9-hour run ($\Delta t = 9$ h), the decay factor, $f = e^{-\lambda \Delta t} = 0.852$, which gives, according to Equation 3,

$$\text{counting factor} = \frac{1 - f}{\frac{0.693}{39\text{ h}}(9\text{h})} = 0.925 \tag{11}$$

The uncertainty rate is calculated is the same manner. The last two columns in Table 6 list the corrected counting rate and the corrected uncertainty rate for each 9-hour run set.

Statistically, for any experiment in which a series of measurements X_i is obtained with corresponding uncertainties δ_i, the average result and average uncertainty can be obtained using the following equations for the weighted average [Mug81]:

$$\bar{X} = \frac{\sum_i \frac{X_i}{\delta_i^2}}{\sum_i \frac{1}{\delta_i^2}} \tag{12}$$

$$\bar{\delta} = \sqrt{\frac{1}{\sum_i \frac{1}{\delta_i^2}}} \tag{13}$$

For the data shown in Table 6, the sum over the 13 sets of data results in an average counting rate of 6.45×10^{-3}/s and an average uncertainty rate of 2.72×10^{-3}/s.

Table 6. 1107-keV peak statistics for first ^{68}Ge experiment.

Run	Total LT (s)	Peak+bkg. area	Total bkg. area	Peak area	Count rate* ($\times 10^{-3}$) (s^{-1})	Uncert. rate ($\times 10^{-3}$)(s^{-1})
1a–9a	21,264	15,596	30,778	207 ± 152.6	10.52	7.75
10a–18a	21,538	11,295	22,314	138 ± 129.9	8.13	7.65
1b–9b	21,664	8277	16,262	146 ± 110.1	10.03	7.57
10b–18b	21,702	6407	12,679	67.5 ± 97.9	5.43	7.85
19b–27b	21.728	5269	10,477	30.5 ± 88.8	2.87	8.38
28b–36b	21.745	4435	8848	11 ± 81.5	1.23	9.02
37b–45b	21,753	3927	7990	−68 ± 77	−8.84	10.0
46b–54b	21.765	3614	7136	46 ± 73.5	7.00	11.2
55b–63b	21,778	3409	6666	76 ± 71.2	13.6	12.7
64b–72b	21,785	3264	6478	25 ± 69	5.25	14.5
73b–81b	21,797	3153	6231	37.5 ± 68.6	9.22	16.9
82b–90b	21,805	3153	6082	112 ± 68.3	32.3	19.7
91b-99b	21,815	3117	6071	81.5 ± 68.1	27.6	23.1

*Counting and uncertainty rates were calculated using the decay and counting factors described in the text..

Table 7. 1077-keV peak statistics for first ^{68}Ge experiment.

Run	Net area of 1077 keV	Count rate (s^{-1})
1a–9a	373,283 ± 721	17.55
10a–18a	372,523 ± 705	17.30
1b–9b	374,706 ± 692	17.30
10b–18b	373,787 ± 687	17.22
19b–27b	372,686 ± 695	17.15
28b–36b	373,595 ± 682	17.18
37b–45b	374,145 ± 672	17.20
46b–54b	372,193 ± 675	17.10
55b–63b	372,867 ± 681	17.12
64b–72b	372,757 ± 660	17.11
73b–81b	374,179 ± 667	17.17
82b–90b	372,814 ± 662	17.10
91b–99b	372,570 ± 668	17.08

From Figure 7, $\epsilon(1107\text{ keV}) = 1.93 \times 10^{-3}$. Using $b(1107\text{ keV}) = 36\%$ and Equation 5, we obtain the activity at the start of measurement (SOM)

$$a_{\text{SOM}}\text{ (Ge-69)} = 9.3 \pm 3.9\text{ /s}$$

Correcting for the decay from the EOB

$$a_{\text{EOB}}\text{ (Ge-69)} = 14.2 \pm 5.97\text{ /s}$$

Flux. The flux is determined from an Fe sample that was irradiated at the same time as the ^{68}Ge solution. A 69-mg sample of natural Fe contains about 0.1932 mg of ^{58}Fe. Using 57.933 g as the atomic mass of ^{58}Fe, the number of ^{58}Fe-atoms in 69 mg of natural Fe is

$$N^{\text{Fe-58}} = 2.01\times10^{18}\text{ atoms}$$

The activity of the ^{59}Fe isotope after bombardment is found by analyzing the areas of the 1099 (57%) and 1292 keV (43%) peaks during a 1371.42 s (*LT*) run. From Figure 7, the efficiencies of the 1099 and 1292 keV peaks are 1.93×10^{-3} and 1.68×10^{-3}, respectively; from Equation 5, the activities at the SOM are 1.46×10^{5} and 1.45×10^{5} /s for the 1099 and 1292 keV peaks, respectively. Using Equation 5 for an 8-h delay, the activities at the EOB are then 1.50×10^{5} and 1.49×10^{5} /s, respectively, for an average of

$$a(^{59}\text{Fe}) = 1.50 \times 10^{5}\text{ /s}$$

Combining these results with the known $\sigma_c = 1.28$ b for ^{58}Fe and $t_{1/2} = 1070.4$ h for ^{59}Fe gives

$$\phi = \frac{1.50 \times 10^{5}\text{ s}^{-1}}{(1.28 \times 10^{-24})(2.01 \times 10^{18})(1 - \exp[\frac{(-0.693)(8\text{ h})}{1070.4\text{ h}}])} = 1.13 \times 10^{13}/\text{cm}^2\text{s}$$

This value agrees very well with the thermal flux estimated for the OSU reactor.

Calculation of N^{68}, the number of ^{68}Ge nuclei. The number of ^{68}Ge nuclei in the sample can be determined by observing the 1077-keV peak in the spectra. The 1077-keV γ ray is a result of the decay chain ^{68}Ge —>^{68}Ga—>^{68}Zn and has a $b(E_\gamma)$ of 2.8%. The net areas and uncertainties of this energy for each of the 13 sets of Ge-a and Ge-b runs is listed in Table 6. The counting rates were calculated using the *LT* sums listed in Table 7. The average counting rate is then 17.2 s^{-1}. From Figure 7, $\epsilon(1077) = 1.93\times10^{-3}$, which implies that the activity of ^{68}Ge is

$$a(1077\ \text{keV}) = \frac{17.2\ \text{s}^{-1}}{(1.93\times10^{-3})(0.28)} = 3.18\times10^{5}\ \text{/s}$$

Using $N = a/\lambda$,

$$N^{68} = 1.08\times10^{13}\ \text{atoms}$$

Calculation of σ_c. From the known activity at EOB, ϕ, and N^{68} and using a decay factor f = exp (–0.693 (8h)/(39h) = 0.867, we can use Equation 5 to find the cross section

$$\sigma_c = \frac{14.2 \pm 6\ \text{/s}}{(1.08\times10^{13})(1.13\times10^{13})(1-0.867)} = 1.13 \pm 0.75\ \text{b}$$

IV.2 Second ^{68}Ge experiment

Unfortunately, the Ge-c series of spectra was accidentally stopped after only 32 iterations. Data sets of 8 runs each (total of four sets) were summed as for the Ge-a and Ge-b data. Table 8 shows the peak area and uncertainty analysis that was calculated in the same manner as the data in Table 6.

Using Equations 12 and 13, the following values of the average count rate and the average uncertainty rate were obtained:

Average counting rate = 1.42×10^{-2} /s

Average uncertainty rate = 4.28×10^{-3} /s

Table 8. 1107-keV peak statistics for second ^{68}Ge experiment.

Run	***LT*** **sum (s)**	**Total bkg**	**Peak+bkg**	**Peak area**	**Count rate (s^{-1})**	**Uncert.rate (s^{-1})**
1c–8c	29,343	44,648	22,792	468 ± 184	0.0225	0.00884
9c–16c	22,467	32,593	16,709	413 ± 158	0.0227	0.00870
17c-24c	22.579	24,168	12,231	147 ± 135	0.00930	0.00854
25c–32c	22649	19,052	9,462	–64 ± 119	0.00465	0.00865

Table 9. 1077-keV peak statistics for second ^{68}Ge experiment.

Run	**Peak Area**	**Count rate (s^{-1})**
1–8c	326,113 ± 639	11.11
9c–16c	327,664 ± 622	14.58
17c–24c	330,447 ± 627	14.64
26c–32c	330,039 ± 617	14.57

Using $\epsilon(1107\ \text{keV}) = 3.3\times10^{-3}$ from Figure 8, Equation 6, and $b(1107\ \text{keV}) = 36\%$,

$$a_{\text{SOM}} = 11.9\pm3.6\ /\text{s}$$

This is the activity of the sample at SOM, that is, at the start of the Ge-c series of runs. This activity is the result of three 8-h irradiations over three days with 16-h nonirradiation periods between each day. Because the $t_{1/2}$ of ^{69}Ge is 39-h, the amount that it decays during these three days is significant. Simply using t_b = 24 h in Equation 5 will not work because the irradiation time is not continuous. Instead, the activity of each irradiation and its subsequent decay to SOM must be summed. By Equation 4, the activity of the ^{69}Ge created during an 8-h irradiation is $a(\text{8-h}) = \phi\,\sigma_c N\,(0.1325)$. By SOM, the activity created each day would have decayed according the exponential decay equation (Equation 1). The decay factor, $f = e^{-\lambda\Delta t}$, of each irradiation period to SOM is then

$$f(\text{first irradiation}) = 0.3084\ (\Delta t = 66.2\ \text{h})$$

$$f(\text{second irradiation}) = 0.472\ (\Delta t = 42.2\ \text{h})$$

$$f(\text{third irradiation}) = 0.724\ (\Delta t = 18.2\ \text{h})$$

Now,

$$a_{\text{SOM}} = \phi\,\sigma_c N^{68}\,(0.1325)\,[0.3084 + 0.472 + 0.724] = \phi\,\sigma_c N^{68}\,(0.1993) \qquad (14)$$

This equation provides σ_c once ϕ *and* N^{68} are determined.

Number of ^{68}Ge nuclei. The net areas of the 1077-keV peak are listed in Table 9. Using $\epsilon(1077) = 3.2\times10^{-3}$ and the *LTs* in Table 8 for each data set, we obtain

$$N^{68} = 5.63\times10^{12}\ \text{atoms}$$

Flux. The 71-mg irradiated Fe sample was analyzed December 21, 1998 at 11:10 for 2814 s (*LT*) without the Pu and Cu absorbing plates. The net areas of the 1099 and 1292 keV peaks were 688,238 and 507,255, respectively. From Figure 8 (top plot), $\epsilon(1099\ \text{keV}) = 3.75\times10^{-3}$ and $\epsilon(1291\ \text{keV}) = 3.7\times10^{-3}$ at the 3-cm position. However, the irradiated Fe

sample was positioned at the 10-cm mark, and there is a 4-cm distance between the detector and the 0-cm mark, so a factor of $(7/14)^2 = 1/4$ must be taken into account in the efficiencies, leading to $\epsilon(1099) = 9.375 \times 10^{-4}$ and $\epsilon(1292\ \text{keV}) = 9.25 \times 10^{-4}$. Using Equation 5 and $b(1099\ \text{keV}) = 57\%$ and $b(1291\ \text{keV}) = 43\%$, the average of the activities at SOM is 4.56×10^5 /s. The decay factor for $\Delta t = 91$ h is $f = 0.943$, so that activity at EOB is 4.84×10^5 /s. The number of ^{58}Fe nuclei in a 71-mg sample is 2.07×10^{18}. Unlike the case for ^{69}Ge, the $t_{1/2}$ of ^{58}Fe is much longer than t_b, the decay factor for a 16-h, nonirradiation time period is approximately 1 ($f = 0.99$), so using $t_b = 24$ h is accurate. Thus,

$$\phi = \frac{4.84 \times 10^5/\text{s}}{(1.28 \times 10^{-24})(2.07 \times 10^{18})(1 - 0.984)} = 1.14 \times 10^{13}$$

which is in good agreement with the value obtained from the first sample.

Calculation of σ_c. Using Equation 14 and the values of a_{SOM}, N^{68}, and ϕ above, we obtain

$$\sigma_c = 0.93 \pm 0.28\ \text{b}$$

In comparison with the value obtained for the first sample of 1.13 ± 0.75 b, the second calculation yields a smaller uncertainty range (0.65 to 1.21 b compared with 0.38 to 1.88 b). It would have been interesting to track the Ge-c series of runs beyond 32 h to see if any of the impurities would have decayed enough to reveal the 1107-keV region better. Also, one is left to speculate how much useful activity was lost after the irradiated sample exploded before being counted.

IV.3 ^{148}Gd experiment.

Complete sample γ*-ray spectra.* The first run (labeled "Gd-b001") to measure the γ-rays emitted from the sample was started at 11:58 on 9 October. This is the SOM time,

t = 43.47 h after EOB. Results of the Gd-b001 run and the Gd-b044 runs are listed in Table 10 for the most easily identifiable γ rays. For each energy, the first row are the net areas and the second row is the number of counts at the peak maximum. The experimental energy is the energy determined from the spectra. For comparison with the expected values, the true energy and its respective branching ratio are provided. The experimental peaks, counts, and net area are in good agreement with the known energies and relative intensities. Those energies marked with an asterisk are the energies from the ^{152}Eu (9 h) isotope; apparently one sample contained a small amount of natural Eu (isotopes ^{151}Eu and ^{153}Eu), which was activated in the reactor. The Gd-b044 run began 11:39 on October 12. An example of the spectra is shown in Figure 12.

Representative peak. The inset of Figure 12 shows the region around the 298 keV peak. This peak had a good shape, was well resolved, and had a relatively strong branching ratio (28.6%). According to Figure 9, the efficiency at 298 keV is 4.7×10^{-3}. The statistics of this peak will be used to monitor the γ-ray activity.

Gamma ray activity of the complete sample. From Table 10, the net area of the 298 keV peak was 566,706 counts in 5286 s at SOM (time when the first spectrum, Gd-b001, was started), making the activity of the complete sample (before first extraction)

$$a_{\mathrm{SOM}}\,(\text{complete sample}) = 7.97 \times 10^4\,/\mathrm{s}$$

Correcting to EOB (Δt = 43.47 h), the activity is

$$a_{\mathrm{EOB}}\,(\text{complete sample}) = 9.12 \times 10^4\,/\mathrm{s}$$

Flux. After irradiation, the 74-mg sample of ^{58}Fe was removed from the poly vial and placed 12-cm from the detector at 13:14 on 13 October and counted for 4906.98 s (*LT*). ^{59}Fe emits two γ rays with energies at 1292 (43%) and 1099 (57%) keV. The spectrum showed a

Table 10. Peak statistics of Gd-b001 and Gd-b044 spectra.

Exp. E (keV)	True E (keV)	b(E_γ)(%)	Gd-b001 (LT = 5286 s)	Gd-b044 (LT = 5590 s)
150.03	149.735	48.2	1,479,695±1344 400,014	1,268,194±1265 334,624
260.68	260.736	1.32	28,247±274 9,341	25,626±275 7,283
272.42	272.321	3.21	70,729±377 18,691	59,241±325 15,261
298.52	298.634	28.63	566,706±859 128,378	479,012±746 113,128
344.19			Double peak 14,764	
346.54			Double peak 92,453	362,526±687 81,831
459.79	459.814	0.579	7743±167 2,505	6747±163 1,801
478.58	478.71	0.23	2552±115 1,545	2606±116 814
496.07	496.383	1.66	23,444±260 5,406	19,928±204 4215
516.42	516.545	2.69	33,928±250 7,555	29,634±235 6065
533.91	534.295	3.07	38,933±274 8,390	33501±232 6984
552.18	552.76	0.086	635±105 1,034	769±94 446
644.82	645.315	1.46	15,632±197 3,505	13,793±138 2509
748.16	748.6	8.22	80,139±349 14,339	67,892±277 11,808
788.35	788.876	7.34	68,001±303 11,888	57,578±252 9738
841.06	841.63*		162,727±438 26,782	
962.67	963.37*		122,948±389 18,980	

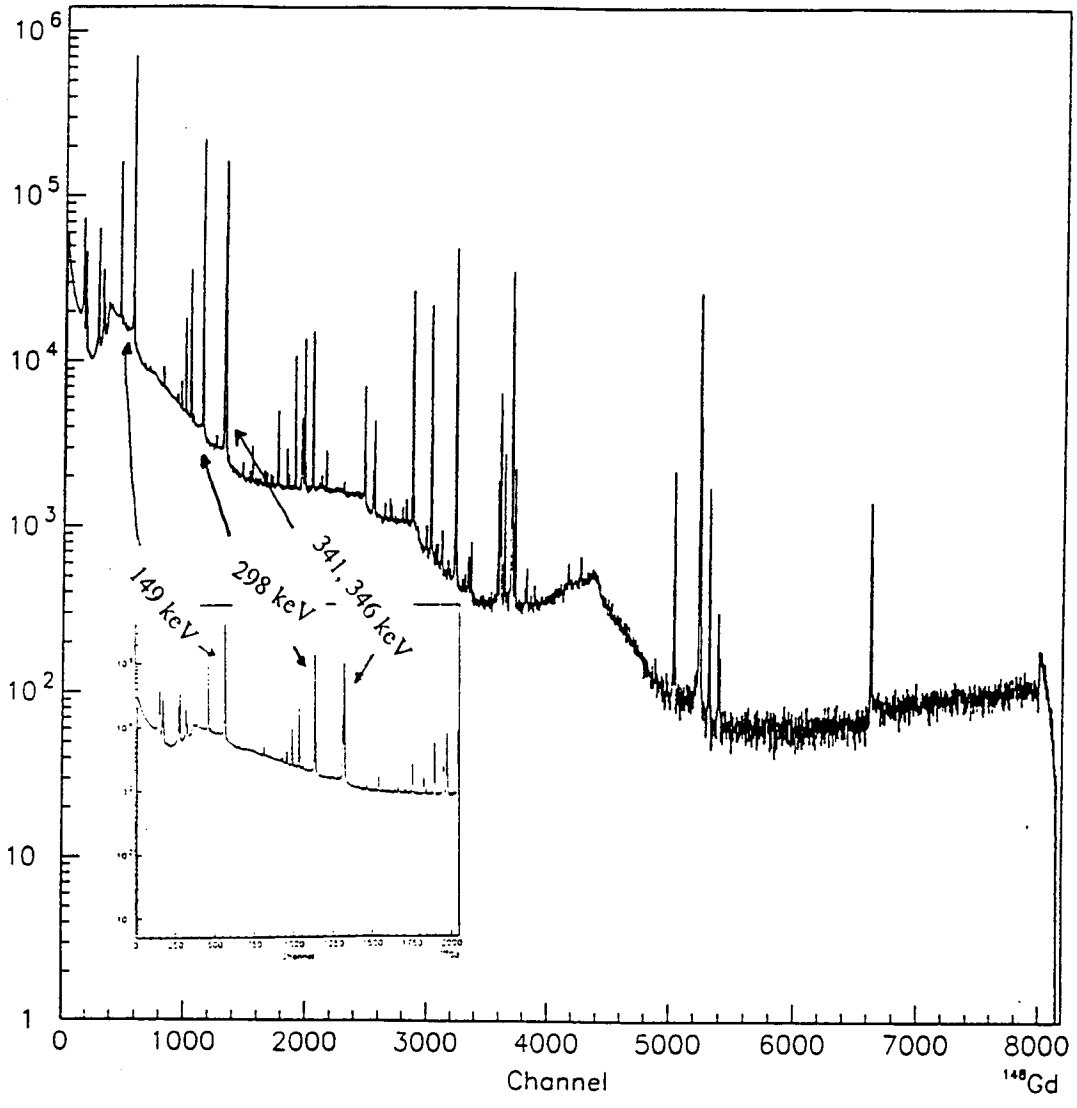

Figure 12. Gamma-ray energy spectrum of irradiated ^{148}Gd.
The inset shows the region about the 298-keV peak.

peak at 1099 keV with a net area of 628, 024±852 and a peak at 1292 keV with a net area of 419,175±659. According Figure 9, the efficiencies at these energies are ϵ(1099 keV) = 1.60×10^{-3} and ϵ(1292 keV) = 1.43×10^{-3}. Therefore, the activities were 1.42×10^{5}/s (from 1099 keV) and 1.38×10^{5}/s (from 1292 keV), for an average of 1.40×10^{5}/s. This is the activity at t = 141 h, and from Equation 1, the the activity at t = 0 was 1.53×10^{5}/s.

Using the same calculation procedure as was used in the ^{68}Ge experiments, a 74-mg sample of natural Fe would have approximately $N^{\text{Fe-58}} = 2.15\times10^{18}$ [a] atoms of ^{58}Fe. Again, the known cross section of ^{58}Fe is 1.28 b and t_b was 8 h, so the flux is

$$\phi = \frac{1.53\times10^{5}}{(1.28\times10^{-24})(2.15\times10^{18})(1-0.995)} = 1.11\times10^{13}\ /\text{cm}^2\text{s}$$

This again is in good agreement with the reported flux of 1.1×10^{13} /cm^{2}s quoted by the OSU Radiation Center.

Activity of the first extracted sample. The dried extracted sample was placed in front of the α detector as described and the activity was measured during a 3600 s (*LT*) run on 14:39, October 14. The spectrum is shown in Figure 10. In the same 84–96 channel ROI as was used for the ^{148}Gd calibration source, the gross area was 8,070 counts. Using the efficiency of the α detector (9.18×10^{-3}), the α-particle activity of the extracted sample is then

$$a_{\alpha}(\text{first extracted sample}) = \frac{8070\ \text{counts}\ /\ 3600\ \text{s}}{(9.18\times10^{-3})(1)} = 2.44\times10^{2}/\text{s}$$

The dried sample was then placed 12 cm from the Ge detector for a γ-ray activity count. A series of 7200-s (real time) runs was begun at 15:49 on October 15. This series was labeled "Gd-c." Results of the first, fifth, and tenth runs are presented in Table 11.

Table 11. Gamma-ray activity of the first extracted sample.

Energy (keV) (keV)	Gd-c001 (LT = 7184 s)	Gd-c005 (LT = 7185 s)	Gd-c010 (LT = 7185 s)
149.77	45,525±240	44,171± 219	42,534±216
260.42	980±55	655±35	~0
298.52	16,783±137	16,276±131	14,777130
747.64	2361±51	2295±50	2238±49
788.09	2056±47	1942±45	1848±45

Table 12. Gamma-ray activity of the second extracted sample.

Energy (keV)	Peak Counts	Net area
149.77	5097	18808±143
260.42	110	268±22
271.90	243	893±35
298.26	1682	7203±88
346.28	1132	5137±76
459.01	28	77±13
495.81	75	295±20
515.64	102	353±23
533.65	103	400±24
644.56	58	151±16
747.64	176	994±33
787.83	124	816±30

The area of the 298 keV peak in the extracted sample at the time of the c001 run was 16,783 counts in 7184 s, making the ^{149}Gd activity of this extracted sample at this time to be

$$a_\gamma(\text{first extracted sample at t = 191.32 h}) = 1.74 \times 10^3 \text{ /s}$$

The γ-ray activity at EOB can be calculated using Equation 1 with Δt = 191.32 h,

$$a_\gamma(\text{first extracted sample at EOB}) = 3.15 \times 10^3 \text{ /s}$$

Determination of N^{148} in the extracted sample. The ^{148}Gd activity of the dried extracted sample was 2.44×10^2 /s, as determined from the α spectrum. The number of ^{148}Gd nuclei in the extracted sample is $N^{148} = a/\lambda$ or

$$N^{148} = (2.44 \times 10^2 \text{ /s})(2.353\ 3\ 10^9 \text{ s}) / 0.693 = 8.28 \times 10^{11} \text{ atoms}$$

where 2.353×10^9 s is the $t_{1/2}$ of ^{148}Gd.

Calculation of σ_c. Using $\phi = 1.11\times10^{13}$ /cm^2 s, $N^{148} = 8.28\times10^{11}$ atoms, and the ^{148}Gd activity of the extracted sample at the EOB of 3.15×10^3 /s, the cross section is

$$\sigma_c = \frac{(3.15 \times 10^3/\text{s})}{(1.11 \times 10^{13}/\text{cm}^2\text{s})(8.28 \times 10^{11})(1 - 0.975)} = 13{,}970 \text{ b}$$

IV.4 Second set of calculations for ^{148}Gd experiment

Second extracted sample. For another calculation of the cross section, a second sample of approximately three drops was extracted, dried, and counted in the same manner as was the first extracted sample.

Gamma-ray activity of the second extracted sample. The γ-ray activity of the second extracted sample was counted in a series of runs labeled Gd-e (Table 12). However, during the counting process, but after the first run, the vial holding the source accidentally moved so

only the results of the first run, Gd-e001 (started 13:38 on October 21, LT = 991.64 s, real time = 6000 s), are shown. Again, the 346 keV peak was not fully resolved owing to a nearby peak from ^{152}Eu, and so its net area value is unreliable.

The γ ray that best represented the spectra was again the 298-keV energy peak (28.6%, $\epsilon = 4.7\times10^{-3}$). Using the data of the 298 keV peak, the ^{149}Gd activity of the second extracted sample from the Gd-e001 run is

$$a_{\gamma}\,(\text{second extracted sample}) = \frac{7203\ \text{counts} / 5991.64\ \text{s}}{(4.7\times10^{-3})(0.2863)} = 8.93\times10^{2}/\text{s}$$

Correcting to EOB (t = 0) using Equation 1 and Δt = 333.14 h, we obtain

$$a_{\text{EOB}}\,(\text{second extracted sample}) = 2.51\times10^{3}/\text{s}$$

Determination N^{148} in the second extracted sample. The second extracted sample was placed in front of the same α detector that was used to count the first extracted sample and at the same position. A new count was started 15:07 on 20 October. After a LT run of 7200 s, the α peak was analyzed using the same ROI channel width (84–96) that was used to analyze the first sample. The gross area was 12,334 counts, making the ^{148}Gd activity of the second extracted sample

$$a_{\alpha}(\text{second extracted sample}) = \frac{12{,}334\ \text{counts} / 7200\ \text{s}}{(1)(9.18\times10^{-3})} = 1.86\times10^{2}/\text{s}$$

Using $N = a/\lambda$, the number of ^{148}Gd nuclei in the extracted source is then

$$N^{148} = \frac{1.86\times10^{2}/\text{s}\,(2.353\times10^{9}/\text{s})}{0.693} = 6.32\times10^{11}\ \text{atoms}$$

where 2.353×10^{9} s is the $t_{1/2}$ of ^{148}Gd.

Table 13. Gamma-ray activity of the irradiated ^{148}Gd after the second sample extraction.

E (keV)	b(E_γ)	Gd-d001 (LT=5780.36 s)		Gd-d10 (LT=5788.80 s)	
		E (keV)	Net area	E (keV)	Net area
149.735	48.2	149.77	670875±861	150.03	644,967±848
260.736	1.32	260.68	12154 ± 153	260.68	12023±150
272.321	3.21	272.16	31635±220	272.16	30176±209
298.634	28.63	298.52	254760±526	298.52	245241±518
346.651*	23.9	346.54	187098±460	346.54	177893±461
459.814	0.579	459.27	3595±85	459.53	3543±89
478.71	0.23	478.32	1261±67	478.32	1340±74
496.383	1.66	495.81	10569±131	469.07	10335±126
516.545	2.69	516.16	15518±147	516.16	14881±143
534.295	3.07	533.65	17394±152	533.91	16813±154
552.76	0.086	552.44	228±37	552.44	263±37
645.315	1.46	644.56	7245±100	644.56	7073±101
748.60	8.22	747.90	36514±198	747.90	35258±197
788.876	7.34	788.09	31290±185	788.09	29512±179
947.835	0.96	946.75	3565±62	946.75	3374±60

* The 346.651 keV peak was a double peak (not well resolved), thus its net area is considered unreliable.

Calculation of σ_c. The flux is the same as in the first calculation ($\phi = 1.11 \times 10^{13}/\text{cm}^2\text{s}$), making the second calculation of the cross section

$$\sigma_c = \frac{2.51 \times 10^3/\text{s}}{(1.11 \times 10^{13}/\text{cm}^2\text{s})(6.32 \times 10^{11})(1 - 0.975)} = 14{,}312\ \text{b}$$

In comparison with the first calculation for the cross section, these values are within 3%. Averaging the two calculated values of the cross section of ^{148}Gd and taking into account a 10% experimental uncertainty, we obtain

$$\sigma_c = 14{,}141 \pm 1414\ \text{b}$$

Spectra accuracy. The γ activity of the liquid sample remaining after the second extraction was measured in a series of spectra runs labeled "Gd-d" (see ^{148}Gd experiment timeline). Table 13 lists the γ-ray intensities of the first and tenth Gd-d runs, Gd-d001and Gd-d010. To verify all the spectra were accurate, the sum of the intensities for each γ ray in the Gd-c series (spectra of first extraction) plus the intensities of each γ ray of the Gd-e series (spectra of second extraction) plus the intensities of each γ ray of the Gd-d series calculated back to the t = 43.7 h time (SOM) should equal the intensities of the Gd-b001 series for each γ ray. The results are shown in Table 14 where the first row represents the net areas at SOM, and the second row for each γ ray are the counts at SOM. The table shows that the results are accurate to within an average of about 12%.

IV.5 Measurement of the upper limit of the (n,p) and (n,α) cross section for ^{148}Gd.

The σ_c of ^{148}Gd is so large that attempts to measure, at the very least, upper limits of the (n,p) and (n,α) cross sections are worthwhile. These reactions usually occur for E_n values higher than those in the thermal region.

Table 14. Peak statistics comparisons to verify spectra accuracy.

E (keV)	Gd-c	Gd-d	Gd-e	Sum	Gd-b001	Difference	(%)
149.74	72,033	1,538,704	46211	1,656,948	1,479,695	177,253	12%
	19,359	417,483	12523	449,365	400,014	49,351	12%
260.74	1551	27,876	658	30,085	28,247	1838	6.5%
	377	8990	270	9637	9341	296	3.2
272.32	3394	72,557	2194	78,145	70,729	7416	10%
	823	19,459	597	20,879	18,691	2188	12%
298.63	26555	584,312	17697	628,564	566,706	61,858	11%
	5949	137,330	4133	147.412	128,376	10,036	15%
459.81	369	8245	189	8,803	7743	1060	14%
	95	2080	69	2,244	2505	–261	10%
516.55	1566	35,592	867	38,025	33,928	4097	12%
	364	7399	251	8,014	7555	459	6%
534.29	1717	39,894	983	42,594	38,933	3661	9%
	403	8346	253	9,002	8390	612	7.3%
645.32	753	16,617	371	17,741	15,632	2109	13%
	153	3140	143	3,436	3505	–69	2%
748.60	3736	83,748	2442	89,927	80,139	9,788	12%
	642	14,649	432	15,723	14,339	1,384	9.6%
788.79	3253	71766	2004	72,023	68,001	9022	13%
	530	11,878	305	12,713	11,888	825	7%

For ^{148}Gd, the process is

$$^{148}\text{Gd} + \text{n} \longrightarrow {}^{148}\text{Eu} + \text{p}$$

^{148}Eu is radioactive with a half life of 54.5 days. It emits a characteristic γ ray with an energy of 550 keV and a branching ration of 98.5%. In December 1998, we accumulated eight additional spectra from the Gd sample to search for the 550-keV γ ray. In the more than 2 months since the irradiation, the strong ^{149}Gd activity (9.3 days) had decayed appreciably, making it possible to search for weak lines from ^{148}Eu. The 550-keV region in the spectrum showed no peak at this energy, so an upper limit defined as $(2\delta)^{1/2}$ (where δ is the gross area of the ROI) was used. A nearby peak was used to find the width of the ROI to be 11-channels. The ratio of the activities of this region to that of the 298-keV peak (from the decay of ^{149}Gd gave an upper limit of the (n,p) cross section to be

$$\sigma(\text{n,p}) < \sigma(\text{n},\gamma)\,(1.8 \times 10^{-5})$$

Using the $\sigma(\text{n},\gamma)$ value obtained above, we obtain

$$\sigma(\text{n,p}) < 0.25\ \text{b}.$$

The (n,α) reaction can written symbolically as follows:

$$^{148}\text{Gd} + \text{n} \longrightarrow {}^{145}\text{Sm} + \alpha$$

The most prominent γ ray is the 61.25-keV γ ray (12.1%). ^{145}Sm has a $t_{1/2}$ of 340 d. Following the same procedure as above, the cross section for the (n,α) reaction is

$$\sigma(\text{n},\alpha) < 9.1 \times 10^{-4}\,\sigma(\text{n},\gamma)$$

Using the value of $\sigma(\text{n},\gamma)$ obtained,

$$\sigma(\text{n},\alpha) < 12.9\ \text{b}$$

V. CONCLUSION

The activation of ^{68}Ge and ^{148}Gd by thermal neutrons has shown to be an effective method for the determination of the neutron capture cross sections. For comparison, Figures 13 and 14 show the σ_c values for some of the isotopes neighboring ^{68}Ge and ^{148}Gd. The elements surrounding ^{68}Ge show cross sections that are also small and of approximately the same order as the 1.03 b obtained in these experiments. The elements surrounding ^{148}Gd, however, are more varied and range from order of 10^{-1} to 10^{4} b.

The difference in the σ_c values between the two nuclei is four orders of magnitude, even though both the ^{68}Ge and the ^{148}Gd were subjected to a neutron flux from the same facility and within the same year. One could reason that the ^{148}Gd nucleus is larger and therefore the strength of the nuclear force is larger, but this still does not explain the enormous difference. What *is* noticeable from Figures 14 and 15 is that adding even one neutron to the nucleus can increase the σ_c values by several order of magnitude. (See, for example, Figure 13 at $_{29}$Cu and neutron numbers N = 34 and 35 and especially Figure 14 at $_{64}$Gd and neutron numbers N = 91 and 92.)

Perhaps the σ_c value for the ^{148}Gd sample represents a resonance, which was generated under the conditions of the reactor. Perhaps there is a resonance in the thermal distribution of velocities of the neutron beam. Either of these reasons could explain the large value for ^{148}Gd obtained in these experiments, although they do not explain the large values for the other Gd isotopes in the figure. If the σ_c values of the elements surrounding the ^{148}Gd and ^{68}Ge isotopes were known, perhaps a pattern would evolve. The existence of a σ_c resonance may be verified in such a case.

	N = 31	N = 32	N = 33	N = 34	N = 35	N = 36	N = 37	N = 38		N = 39	N = 40		N = 41
$_{36}$Kr													
$_{35}$Br													
$_{34}$Se											52 *1*		
$_{33}$As													
$_{32}$Ge						1.03		3.15 *16*	0.28 *7*		0.98 *9*		15 *2*
$_{31}$Ga								1.68 *7*			4.7 *2*	0.1 *1*	
$_{30}$Zn				0.76 *2*		0.85 *20*	6.8 *8*	1.0 *1*	0.072 *4*		0.092 *5*		
$_{29}$Cu				4.50 *2*	6 *2* E3	2.17 *3*	135 *10*						
$_{28}$Ni	78 *4*	2.9 *2*	2.5 *8*	14.5 *3*	24 *3*	1.52 *3*	22.4 *2*						

Figure 13. σ_c values of isotopes neighboring ^{68}Ge.

	N = 82	N = 83	N = 84	N = 85	N = 86	N = 87	N = 88	N = 89	N = 90	N = 91	N = 92
$_{68}$Er											
$_{67}$Ho											
$_{66}$Dy									33 *3*		43 *6*
$_{65}$Tb											
$_{64}$Gd			1.4 *1* E4				735 *20*	3.6 *4* E4	85 *12*	6.1 *1* E4	1.5 *1* E3
$_{63}$Eu							5.9 *2* E3	1.3 *1* E4	312 *7*	1.3 *1* E3	4.0 *1* E3
$_{62}$Sm	0.7 *3*	≈ 220		57 *3*	2.4 *6*	4.0 *1* E4	104 *4*	1.523E4	206 *6*	420 *180*	8.4 *5*
$_{61}$Pm				8 *2* E3	96 *2* / 72 *3*	2 *1* E3	1.4 *3* E3		< 700		
$_{60}$Nd	18.7 *7*	325 *10*	3.6 *3*	42 *2*	1.4 *1*	440 *150*	2.5 *2*		1.2 *2*		

	N = 92	N = 93	N = 94	N = 95	N = 96	N = 97	N = 98		N = 99	N =100	N =101	N =102
$_{68}$Er			19 *2*		13 *2*		5 *3*	15 *2*	659 *16*	2.74 *8*		5.8 *3*
$_{67}$Ho							61 *1*	3.5 *4*				
$_{66}$Dy	43 *6*		56 *5*	600 *25*	194 *10*	124 *7*	1040 *140*	1610 *240*	3.6 *3* E3 / 2.0 *6* E3			
$_{65}$Tb			23.4 *4*	525 *100*								
$_{64}$Gd	1.5 *12*	2.54*1* E5	2.2 *2*		0.77 *2*	3.1*12*E4						
$_{63}$Eu	4.0*1* E3											
$_{62}$Sm	8.4 *5*											
$_{61}$Pm												
$_{60}$Nd												

Figure 14. σ_c values of isotopes neighboring ^{148}Gd.

Then, there is also a possibility that the σ_c value we calculated for ^{148}Gd actually represents the cross section of more than just an (n,γ) reaction. If so, the upper limits of the (n,p) and (n,α) cross sections calculated in section IV.5 may be much too small, and the 550- and 61-keV lines are really more intense than our spectra showed. Measuring the absorbtion cross sections of all n-capture processes would resolve this and leaves room for experimentation.

The inability to visibly analyze the peaks of irradiated ^{68}Ge, has lead to proposals for future experiments. If the irradiation time can be extended for continuous bombardment and/or if the flux can be increased, the ratio of the peak intensity of the 1107-keV energy to the background impurities may be increased. During the analysis, it was determined that a majority of the background results for a strong impurity which seemed to decay rapidly after 15 h. This fact, plus the presence of a strong peak at 1368-keV indicates that the impurity may be ^{24}Na. Because the impurity reaches its saturation point before (and more rapidly) than ^{69}Ge, long irradiations will only increase the amount of ^{69}Ge present while keeping the background constant. Also, if the flux could be increased to, say, orders of 10^{14}, the increase in the number of neutrons available for capture also could increase the peak's intensity. Currently, the University of Missouri provides such experimental conditions. However, limitations still exist in that the sample must be solid and in that there is no risk that the explosion that occurred in the second Ge experiment will happen.

In spite of our inability to see the ^{69}Ge energy spectra clearly or to justify the large value obtained for ^{148}Gd, these results still provide an insight into the processes leading to thermal neutron capture and provide useful information on which to base future experimentation.

BIBLIOGRAPHY

All84 B.J. Allen, "Theory of Slow Neutron Radiative Capture," in *Neutron Radiative Capture,* Neutron Physics and Nuclear Data in Science and Technology Vol. 3, R.E.Chrien, Ed. (Pergamon Press, New York, 1984), Chapter 1, pp. 1–32.

Cla68 D.D. Clayton, Principles of Stellar Evolution and Nucleosynthesis (McGraw-Hill, New York, 1968), pp. 546–591.

Chr84 R.E. Chrien, "Practical Uses for Neutron Capture Gamma-Ray Spectroscopy," in *Neutron Radiative Capture,* Neutron Physics and Nuclear Data in Science and Technology Vol. 3, R.E.Chrien, Ed. (Pergamon Press, New York, 1984), Chapter VII, pp. 187–213

Cur59 I.F. Curtiss, *Introduction to Neutron Physics* (Technical Publisher, Boston, MA, 1959).

Ejn98 R. Ejnisman, I.D. Goldman, K.S. Krane, P. Mohr, Y. Nakazawa, E.B. Norman, T. Rauscher, and J. Reel, "Neutron Capture Cross Section of ^{44}Ti," *Phys. Rev. C* **58**, 2531 (1998).

Fai79 K.P. Failey, D.L. Anderson, W.H. Zoller, and G.E. Gordon, "Neutron Capture Prompt Gamma Ray Activation Analysis for Multielement Determination in Complex Samples," *Anal. Chem.* **51,** 2209 (1979).

Fir96 R.B. Firestone and V.S. Shirley, *Table of Isotopes* (Wiley, New York, 1996).

Kob82 T. Kobayashi and K. Kanda, "Analytical Calculation of Boron-10 Dosage in Cell Nucleus for Neutron Capture Therapy," *Rad. Res.* **91,** 77 (1982).

Kra88 K.S. Krane, *Introductory Nuclear Physics* (John Wiley & Sons, New York, 1988).

Lyn 68 J.E. Lynn "Radiative Capture," in *The Theory of Neutron Resonance Reactions* (Claredon Press, Oxford, UK, 1968), Chapter VII, pp. 291.

Mer19 *Merck Index,* 11th ed., S. Budavari, Ed (Merck & Co., Inc., Rahway, NJ, 1989).

Mug81 S.F. Mughabghab, M. Divadeenam, and N.E. Holden, Neutron Cross Sections, Resonance Parameters and Thermal Cross Sections (Academic Press, Inc., New York, 1981).

BIBLIOGRAPHY, CONTINUED

Poe84 W.P. Poenitz, "Measurement Techniques for Radiative Neutron Capture," in *Neutron Radiative Capture,* Neutron Physics and Nuclear Data in Science and Technology Vol. 3, R.E. Chrien, Ed. (Pergamon Press, New York, 1984), Chapter IV, pp.119–153.

Sch60 H.W. Schmitt and C.W. Cook, "Absolute Neutron Absorption Cross Sections for Sb-Be Photoneutrons," *Nucl. Phys.* **20,** 202 (1960).